Energy Reports 9 (2023) 4437–4455

Contents lists available at ScienceDirect

Energy Reports

journal homepage: www.elsevier.com/locate/egyr

Research paper

Sensitivity analysis and multi-objective optimization of the energy, exergy and thermo-economic performance of a Brayton supercritical CO_2-ORC configurations

Guillermo Valencia Ochoa [a,*], Dora Villada Castilla [b], Daniel Mendoza Casseres [c]

[a] Efficient Energy Management Research Group, Mechanical Engineering Department, Universidad del Atlántico, Carrera 30 Número 8-49, Puerto Colombia 080007, Colombia
[b] Faculty of Engineering, Universidad Francisco de Paula Santander, Cucuta 540003, Colombia
[c] Research Group 3i+d, Industrial Engineering Department, Universidad del Atlántico, Carrera 30 Número 8-49, Puerto Colombia 080007, Colombia

ARTICLE INFO

Article history:
Received 18 May 2022
Received in revised form 21 February 2023
Accepted 19 March 2023
Available online 25 March 2023

Keywords:
Brayton
Supercritical CO_2
Simple organic Rankine cycle
Regenerative organic Rankine cycle
Thermo-economic
Multi-objective optimization

ABSTRACT

The following research compared some energy, exergetic and thermo-economic indicators of a supercritical CO_2 simple Brayton cycle integrated with a simple organic Rankine cycle (SORC), and a regenerative organic Rankine cycle (RORC). A thermodynamic model was developed to determine the net power, thermal efficiency, the fuel consumption, and the exergy destruction of all the components of the system. Also, a thermo-economic model was developed to determine some economic indicators such as the levelized cost of energy (LCOE), the payback period (PBP) and specific investment cost (SIC). A sensitivity analysis was carried out to study the influence of the primary turbine inlet temperature (TIT), the high-pressure in the compressor (P_{High}), the evaporator pinch point temperature difference (PPT), and the pressure ratio (P_r) on the indicators performance. Three different working fluids were selected in this study: acetone, toluene and cyclohexane. The results showed that cyclohexane had the best energy performance giving an efficiency of 48.02% for the RORC system. Besides, it presented the best thermo-economic results for the LCOE (0.26 USD/kWh), SIC (2626.75 USD/kWh), and a PBP (11.2 years). Finally, a multi-objective optimization was developed based on energy, exergy and thermo-economic performance parameters as objective functions to obtain a technical and economic feasible solution able to implement them in industrial applications.

1. Introduction

Industry currently has different heat transfer mechanisms in its productive processes. In the sector of power generation, the production of exhaust gases released to the environment has become a problem because of the loss of energy and air pollution (Jaber et al., 2017). Between the 60%–70% of the primary energy is lost as low-grade waste heat.

The loss of energy due to unused waste of heat contributes to the increase in production costs and cause environmental damage. The cost of energy represents a significant part of the total cost of production of a variety of consumer goods. In recent years, different methods have been investigated to optimize the energy generation and consumption systems, considering increased efficiency and minimization of facility costs (Uusitalo et al., 2019; Khaled et al., 2020). These alternatives include the use of waste heat, which can provide significant improvements in overall efficiency and reduce greenhouse gas emissions in energy production systems and industrial processes (Sara et al., 2018; Young et al., 2018).

In addition to the residual heat generated in industrial processes, there are other energy resources in the world such as geothermal and solar energy. These are called low-quality energy resources because they are sources at low temperatures (Boullaga et al., 2017; Thakar et al., 2018; Benato et al., 2017; Sukumaran and Sudhakar, 2018). Conventional power generation techniques are not efficient in converting heat from traditional sources. Therefore, due to the low temperature generated by these electrical energy sources, many scientists have turned their attention to the use of waste of heat because it has low enthalpy, lower costs than high-temperature heat and is abundant in industrial process (Mostafavi and Mahmoudi, 2018).

Several thermodynamic cycles have been proposed for energy conversion from residual heat recovery (Danieli et al., 2019; Dudkiewicz and Szałański, 2020; Nami et al., 2018). However, many of these conventional steam cycles are not efficient when using low-quality waste heat recovery. Therefore, the ORC represents an

* Corresponding author.
E-mail address: guillermoevalencia@mail.uniatlantico.edu.co (G.V. Ochoa).

https://doi.org/10.1016/j.egyr.2023.03.102

effective alternative to use energy because of its low-temperature heat recovery capacity and the possibility of being implemented in low capacity and decentralized plants (Imran et al., 2018). ORC systems offer an attractive option for geothermal energy exploitation. Besides, there is extensive research available in this field, including work fluid selection, component design, cycle optimization, thermal, exergetic, economic, and environmental impact assessment (White and Sayma, 2019; White et al., 2017, 2018; Tartière and Astolfi, 2017; Arbolino et al., 2017; Xia et al., 2020).

The exergetic and thermo-economic analysis has become a useful tool for quantifying cycle inefficiencies and identifying whether the energy consumption is optimal or not, enabling crucial information for system design and operation (Sánchez Villafana and Vargas Machuca Bueno, 2019). In this sense, Hou et al. (2020), made an exergo-economic analysis of an ORC cycle through the TLEEA (Three-Level exergo-economic Assessment) method, calculating the assessment indicators using a correlation matrix. Their results were focused on a typical system operation that makes it necessary to investigate the variation in economic performance based on different operating parameters. Although the ORC cycle is commonly applied in many waste heat recovery processes, it still has some limitations when residual heat is at high temperatures due to the different thermophysical properties of organic fluids. For this reason, several studies have been done about the combination of the ORC cycle with other thermodynamic cycles to improve its efficiency, such as the S-CO_2 Brayton cycle. Compared to other thermodynamic cycles, the S-CO_2 Brayton cycle has a higher economic advantage because it employs more compact components due to the high operating pressure and density of S-CO_2. Also, the cycle is favorable for the selection of structural materials of the components.

Several researchers proposed the use of the organic Rankine cycle as a low temperature was heat recovery system from S-CO_2 Brayton cycle (Teng and Xuan, 2019; Zhou et al., 2018; Noaman et al., 2019; Novales et al., 2019; Qiao et al., 2020; Ochoa et al., 2022; Valencia Ochoa et al., 2020), also the thermo-economic and performance optimization had been considered considering some performance indicators (Ochoa et al., 2022; Valencia Ochoa et al., 2020). In this sense, Abrosimov et al. (2019) employed a combination between the supercritical Brayton cycle and an ORC cycle through computational models. The thermo-economic optimizations allowed to compare the different solutions to show that the combined scheme has a 10% increase in the overall system efficiency and a 6% decrease over the Levelized Cost of Energy (LCOE). Cao et al. (2022) performed a thermodynamic analysis and optimization of a supercritical CO_2 recompression Brayton cycle coupled to ORC driven by solar and geothermal energy. The optimization showed that the optimal thermal efficiency of the cycle reached 35.07%. Similar work was carried out by Khademi et al. (2022) who performed a multi-objective thermo-economic optimization of a solar-assisted supercritical CO_2 Brayton cycle integrated to an ORC cycle using solar energy as the thermal source. The results of the optimization showed that the maximum exergy efficiency of the combined system was 61.7% and the minimum cost of electricity production was 0.2617 $/kWh. Habibi et al. (2020) carried out an optimization of a regenerative supercritical Brayton cycle integrated with a simple organic Rankine cycle (SORC) driven by a concentrating solar power (CSP) tower. The results showed that implementing the ORC cycle increased the net power's system power (2.75%) and the exergy efficiency (2.16%) using helium as the working fluid. Song et al. (2018) adapted a supercritical Brayton cycle with a recuperator coupled to an ORC for heat recovery. The results showed that integrating the ORC cycle into the Brayton cycle generated a percentage increase of 1.3% as compared to the Brayton cycle without ORC. Studies oriented towards the exergo-economics optimization of combined supercritical Brayton cycle and organic Rankine cycle using zeotropic mixture fluid were carried out by Hou et al. (2018). In this work the researchers proposed different Brayton configurations and zeotropic mixture. Among the main results, the optimal zeotropic mixture was R236fa/R227ea (046/0.54). In addition, the optimum values of exergy efficiency and total product unit cost are found to be 73.65% and 10.93 $/GJ, respectively. Finally, Liang et al. (2020) performed a simultaneous optimization of combined supercritical Brayton cycle and organic Rankine cycle integrated with concentrated solar power system. The authors concluded that the integration of the ORC cycle increased the thermal efficiency by 3.6–4.4% compared with the literature results.

Studies have been focusing in thermo-economic multi-objective optimizations of standard and regenerative ORC, founding the behavior of economics variables in different heat source types. However, the study have not found the optimal operational conditions where the systems presents both the highest output power and exergetic efficiency as the lower specific investment cost (Braimakis and Karellas, 2017). On the other hand, there is an investigation that the objective of the optimization was to obtain the highest exergy efficiency looking for a minimum pressure ratio, and pinch point temperature, but it was limited only to a ORC system, and the result was compared to the best performance of ORC systems with recuperator with the lowest SIC getting the highest exergy efficiency (de Campos et al., 2020).

The main contribution of this paper is to present the energy, exergy and thermo-economic parametric study and multi-objective optimization of two S-CO_2-ORC Brayton configurations, based on thermal and economic performance indicators such as the net output power, the payback period, the levelized cost of energy, and the specific investment cost. Although previous studies have proposed improvements in the performance of waste heat recovery systems through the organic fluid selection, the exergo-economic analysis and the improvement of equipment characteristics; there are few investigations developed in relation to the combination of ORC as bottoming cycle from S-CO_2 Brayton cycles evaluated through a systematic approach, particularly considering thermal and thermo-economic criteria, involving a multi-criteria optimization. Therefore, these results can be considered as a fundamental basic in the continue search of technical and economic feasible solution.

2. Methodology

2.1. System operation

Fig. 1a shows the configuration of combined supercritical CO_2 simple Brayton cycle with simple organic Rankine cycle (SORC, Fig. 1a), and regenerative organic Rankine cycle (RORC, Fig. 1b). This study two ORCs were proposed to evaluate the performance of the system, and analyze the heat recovery of the combined cycle. It is done to optimize the overall thermal efficiency of the arrangement to have better use of energy. The configurations proposed in Fig. 1 consist of three coupled circuits. The first circuit consists of the supercritical CO_2 simple Brayton cycle. The second circuit was called the thermal oil circuit (secondary circuit). This circuit is designed to absorb the waste heat from the CO_2 using a high heat transfer oil (Therminol 66). In addition, this circuit makes it possible to counteract pressure drops that may occur in the Brayton and thus ensure the integrity of the ORC cycle equipment. A third circuit, consisting of waste heat recovery technologies, using organic Rankine cycle.

The supercritical CO_2 Brayton cycle layout uses an axial compressor (C1) that compresses the gas (or CO_2) and sends it to

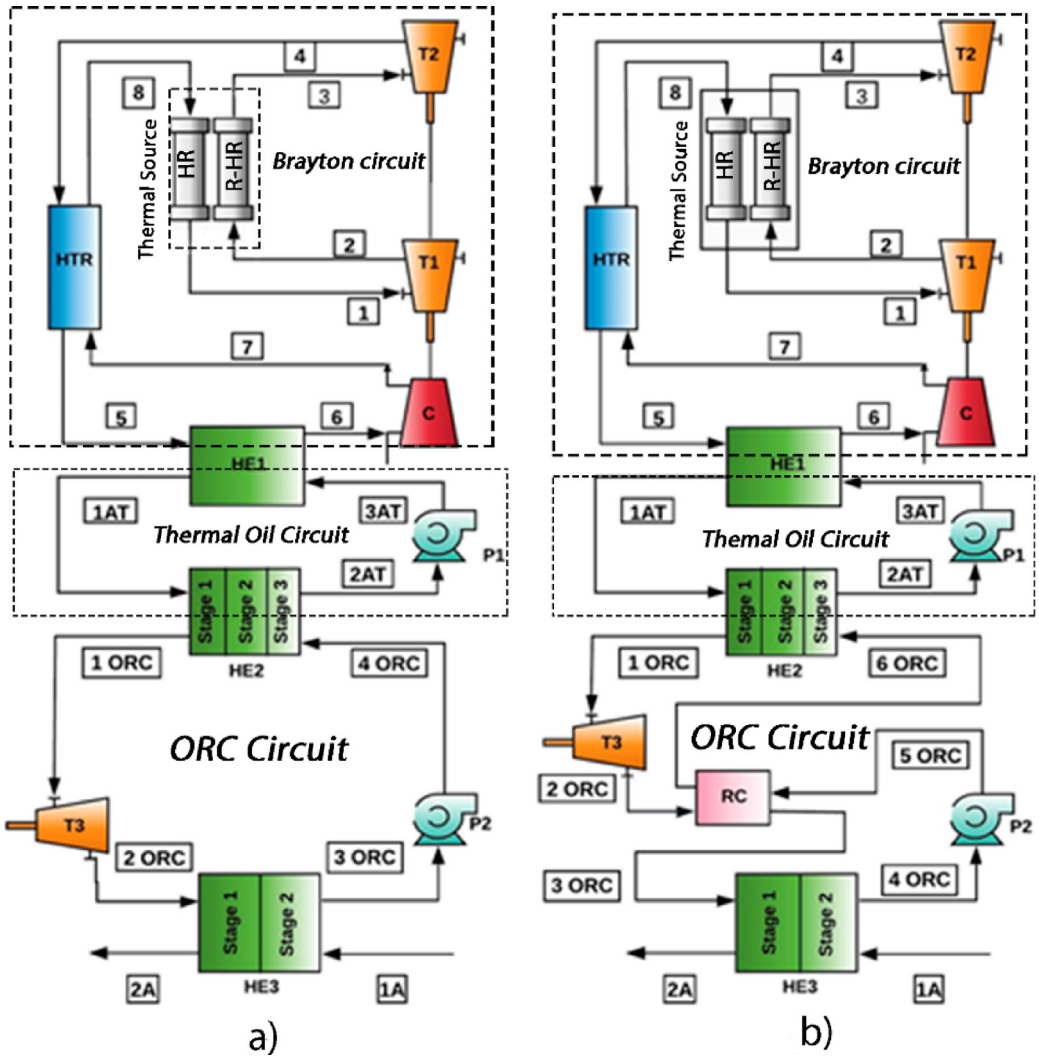

Fig. 1. Physical structure for the cycles: (a) S-CO_2 – SORC Brayton cycle, and (b) S-CO_2– RORC Brayton cycle.

the primary turbine (T1), and secondary turbine (T2). The CO_2 is heated in the heater (HR), and then enters the turbine (T1) where it expands to generate power output. Next, the CO_2 is reheated in the reheater (R-HR) that increases the temperature to then enter the turbine (T2). Subsequently, the hot stream from the turbine (state 4) passes through the high temperature recuperator (HTR), to recover part of the heat and preheat the air coming from the compressor (state 7). Then, the CO_2 enters to the plate and shell heat exchanger (HE1) that is coupled with the organic Rankine cycle to be cooled. The secondary thermal coupling circuit uses a high-heat transfer oil (Therminol 66). The thermal oil absorbs the heat from the carbon dioxide in the shell and tube heat exchanger (HE1), avoiding direct contact between the heat source and the ORC working fluid. This ensures better thermal stability of the organic fluid. Subsequently, the thermal oil is pumped through the pump (P1) towards the ORC plate evaporator (HE2).

The plate evaporator (HE2) increase the temperature of the working fluid in three stages (heating, evaporation, overheating). The goal of this process is to transfer the remaining heat to the organic fluid of the ORC. After receiving the heat, the organic fluid moves to the turbine (T3) used in the ORC to expand and decrease high temperature and pressure. During the process the fluid generates power and reaches the required properties to enter the condenser (HE3). Here, the fluid exchanges heat with an external source of water (state 1A) to reduce its temperature. In the case of the RORC configuration (Fig. 1b) the fluid that leaves the turbine (T3) enters to a heat recovery (RC). Then, the organic fluid goes to the heat exchanger (HE3) and leaves it as saturated liquid (state 4 ORC), and it is pumped by the secondary pump (P2) of the configurations. The objective of the combined cycle is to increase the thermal performance of the S-CO_2 Brayton cycle by mean of the use of the organic Rankine cycle configurations as bottoming cycles. The heat transferred between the cycles produces steam that is sent to the turbines generating higher net power in the system. Such configurations are essential because their components have high availability in the market. They also have economic advantages in energy use, causing an increase in energy efficiency by recovering the heat generated in the processes.

Fig. 2 shows the entropy diagrams of the S-CO_2- SORC Brayton cycle (Fig. 2a) and S-CO_2 - RORC Brayton cycle (Fig. 2b). It lets to analyze the temperature of the process development and identify the availability of useful energy. For the development of the S-CO_2-SORC Brayton cycle, the working fluid enters the primary turbine and secondary turbine with high-temperature and entropy (state 1 and state 3). It lets the best use of the turbine under these conditions and causes the cycle to have a significant loss of energy. The fluid is sent to the HTR, where the fluid exchanges heat with the fluid of the ORC system.

Then, the fluid is distributed throughout the system configuration for the two case studies. Its residual percentage in the

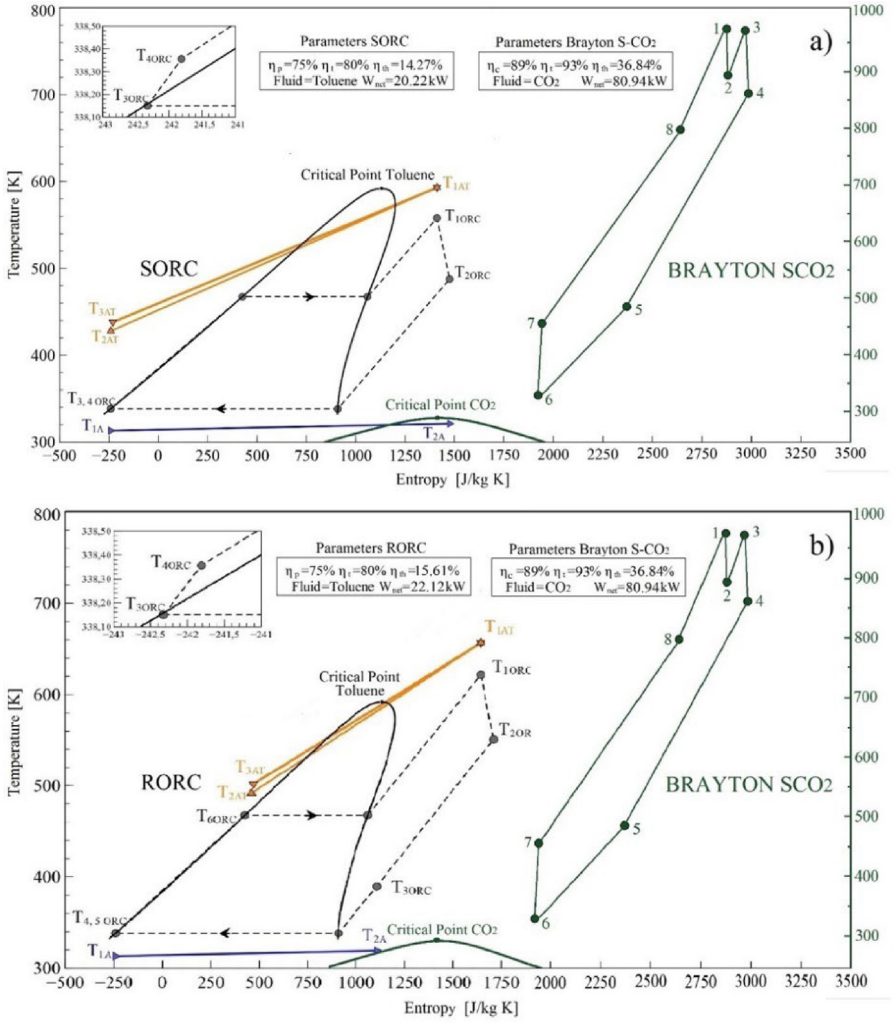

Fig. 2. T–S diagram for the layouts: (a) S-CO_2- SORC Brayton cycle, and (b) S-CO_2 – RORC Brayton cycle.

S-CO_2 Brayton cycle is recirculated through a heat exchanger that supplies heat to the system and a compressor. It transfers enough energy to be used in the turbines. It can be seen a decrease in temperature and fluid entropy between the states 1AT and 2AT, in the simple organic Rankine cycle. It happens because the working fluid transfers energy in the HE2 to the organic fluid that activates the ORC turbine. Because of the decrease in temperature and entropy in the HE3, the fluid gets condensed. Then, it is propelled by the P2 secondary pump to be recirculated in the two systems.

Fig. 2b shows the T–S diagram for the S-CO_2–RORC Brayton cycle. For this configuration, the working fluid of the ORC cycle experiences two more states than in the simple configuration. It happens because the heat recovery incorporated into the system exchanges the residual heat of turbine-3 with the fluid that is recirculated from the secondary pump (P2). It increases the temperature of the organic working fluid, which is sent to the Brayton cycle.

2.2. Organic working fluid selection

In this section, it was selected fluids with thermo-physical properties compatible with the cycles, as well as with low environmental impact. Table 1 shows the criteria used to select the working fluids. It was done to evaluate its properties and analyze its performance in the configurations studied (Rahbar et al., 2017). It is pertinent to emphasize that it is not within the scope of this work to make a detailed selection or to present a selection methodology.

The Table 2 shows the thermo-physical and environmental properties of some commonly used ORC fluids. The dry and isentropic organic fluids widely used in the organic Rankine cycles, were selected with the criteria considered in Table 1 (Shi et al., 2018; Kölsch and Radulovic, 2015; Grelet et al., 2016). Among them are some alkanes, siloxanes, and refrigerants. Chlorofluorocarbons (CFCs) and hydrochlorofluorocarbons were not included as candidates because of their environmental effects according to the Montreal Protocol (Secretariat, 2000) as well as hydrofluorocarbons (HFCs) because of their high GWP values according to the Kyoto Protocol (Anon, 1998). In this work, high priority was given to environmentally friendly fluids with high thermal stability. In this sense, and based on previous studies in ORC (Grelet et al., 2016; de Oliveira Neto et al., 2016), toluene, acetone and cyclohexane were selected as the working fluids.

2.3. Thermodynamic model

The following considerations detailed below were considered for the development of the thermodynamic model studied in the described configurations of the two Brayton cycle systems, without heat recovery and with heat recovery. The numerical model development was developed in Matlab R2015. The thermophysical and transport properties of the fluids were obtained from REFPROP 9.1 linked with Matlab.

Table 1
Organic working fluids selection criteria.

No	Criteria	Operational parameter	Observation	Reference
1	Critical temperature	> 250 °C	To allow condensation of the working fluid	Invernizzi et al. (2007)
2	Slope of the saturated steam curve	$\varepsilon > 0.5$ (dry) $\varepsilon < -0.5$ (wet) $-0.5 \leq \varepsilon \leq 0.5$ (isentropic)		Maizza and Maizza (1996), Michos et al. (2017)
3	Global Warming Potential (GWP)	<2000	The design criterion prefers fluids with GWP equal to or less than 2000	Desai and Bandyopadhyay (2009), Ambiente and Territorial (2008)
4	Ozone Depletion Potential (ODP)	0	It should be equal to zero	Desai and Bandyopadhyay (2009)
5	Safety classification (NFPA 704 standard)	Class 4 not allowed	According to the standard NFPA 704 the fluid must not be in safety class 4, because it would present a maximum level of flammability	Anon (2017)

Table 2
Properties of dry and isentropic organic fluids.

Fluid	Molecular mass (kg/kmol)	T_{crit} (°C)	P_{crit} (kPa)	GWP (Low/<2000)	Type of fluid (ξ)	ODP	NFPA 704	
							Flammability	Health risk
Cyclohexane	84,2	280	4082	Low	Dry (1.78)	0	3	1
D4	296,6	313	1332	-	Dry (2.38)	0	–	–
D5	370,8	346	1160	-	Dry (2.54)	0	2	1
D6	444,9	373	961	-	Dry (2.90)	0	–	–
Heptane	100,2	267	2736	LLow	Dry (2.61)	0	3	1
Hexane	86,2	235	3034	Low	Dry (2.25)	0	3	2
Isohexane	86,2	225	3040	Low	Dry (2.33)	0	3	1
MD2M	310,7	326	1227	-	Dry (2.80)	0	2	1
MD3M	384,8	355	945	-	Dry (3.04)	0	2	1
MD4M	459,0	380	877	-	Dry (2.82)	0	0	0
MDM	236,5	291	1415	-	Dry (2.89)	0	3	0
Toluene	92,1	319	4126	2.7	Isentropic (1.22)			
Acetone	58.08	235	3780	0.5	Isentropic (0.31)	0 0	3 3	2 2
i-butane	58,18	135	3640	20	(0.48)	0	4	1
R-245fa	134,05	154	3640	1030	Isentropic (0.34)	0	0	2

- All components are open systems.
- Changes in kinetic and potential energies are negligible (Kim et al., 2012).
- Ambient temperature of 25 °C.
- Ambient pressure of 101.3 kPa.
- Turbines were considered isentropic and adiabatic.
- The pressure drops in the heat exchangers are assessed considering the geometry and the flow rate.
- The pressure drop was not included in the pipe system.
- Pressure drops due to friction were negligible (Kim et al., 2012).
- The effectiveness of HTR is considered (Sarkar, 2009).

The efficiency of the system was calculated using the first law of thermodynamics, is define by Eq. (1).

$$\eta_I = \frac{\dot{W}_{net,\text{Brayton}} + \dot{W}_{net,\text{ORC}}}{\dot{Q}_{HR} + \dot{Q}_{R-HR}} \tag{1}$$

where $\dot{W}_{net,\text{Brayton}}$ is the net power generated by the Brayton system, $\dot{W}_{net,\text{ORC}}$ is the power generated by the ORC cycle, $\dot{Q}_{HR}$ and $\dot{Q}_{R-HR}$ are the heats supplied by the heater and the reheater, respectively.

The net power of the Brayton cycle can be calculated by Eq. (2).

$$\dot{W}_{net,\text{Brayton}} = \dot{W}_{T1} + \dot{W}_{T2} - \dot{W}_{C1} \tag{2}$$

where $\dot{W}_{T1}$ and $\dot{W}_{T2}$ are the power generated by the turbines (T1) and (T2), and $\dot{W}_{C1}$ is the power of the compressor (C1).

On the other hand, the calculation of the net power generated in the ORC cycle was determined by Eq. (3).

$$\dot{W}_{net,ORC} = \dot{W}_{T3} - \dot{W}_{P1} - \dot{W}_{P2} \tag{3}$$

where $\dot{W}_{T3}$ is the power of the turbine (T3), $\dot{W}_{P1}$ is the power of the pump (P1) and $\dot{W}_{P2}$ is the power of the pump (P2).

The thermal efficiency of the S-CO_2 Brayton cycle is given by Eq. (4).

$$\eta_{I,\text{Brayton}} = \frac{\dot{W}_{net,Brayton}}{\dot{Q}_{HR} + \dot{Q}_{R-HR}} \tag{4}$$

where $\dot{W}_{net,Brayton}$ is the net power of the S-CO_2 Brayton cycle. $\dot{Q}_{HR}$ and $\dot{Q}_{R-HR}$ are the heats supplied by the thermal source. The thermal source is conformed by a heater (HR), and reheater (R-HR).

The thermal efficiency of the ORC system is determined by Eq. (5).

$$\eta_{I,ORC} = \frac{\dot{W}_{net,ORC}}{\dot{Q}_{HE1}} \tag{5}$$

where $\dot{W}_{net,ORC}$ is the net power of the ORC system and $\dot{Q}_{HE1}$ is the energy transferred in the heat exchanger (HE1).

Finally, the overall efficiency of the S-CO_2–ORC Brayton system can be calculated by Eq. (6).

$$\eta_{I,overall} = \frac{\dot{W}_{net,Brayton} + \dot{W}_{net,ORC}}{\dot{Q}_{HR} + \dot{Q}_{R-HR}} = \frac{\dot{W}_{net,Brayton} + \dot{W}_{net,ORC}}{\dot{m}_{CO2} \cdot [(h_1 - h_8) + (h_3 - h_2)]} \quad (6)$$

The absolute increase of the efficiency of the S-CO_2-ORC Brayton system ($\Delta\eta_{th}$) considering the efficiency of the S-CO_2 Brayton cycle, can be calculated by Eq. (7).

$$\Delta\eta_{th} = \frac{\dot{W}_{net,ORC}}{\dot{Q}_{HR} + \dot{Q}_{R-HR}} \quad (7)$$

The exergetic efficiency of the entire configuration is determined by Eq. (8).

$$\eta_{II} = \frac{\dot{W}_{net,\mathrm{Brayton}} + \dot{W}_{net,\mathrm{ORC}}}{\dot{E}_{in}} \quad (8)$$

where $\dot{E}_{in}$ is the exergy given to the thermal source, which is determined by Eq. (9).

$$\dot{E}_{in} = (\dot{Q}_{HR} + \dot{Q}_{R-HR}) \cdot \left(1 - \frac{T_0}{TIT}\right) \quad (9)$$

where T_0 is the ambient temperature, and TIT is the turbine inlet temperature. The inlet temperature of the turbines, main turbine (T1) and secondary turbine (T2), are equal. To achieve this, the thermal source (HR plus R-HR) must supply the heat necessary to increase the CO_2 temperature, according to Eq. (10).

$$\dot{Q}_{tm} = \dot{m}_{CO2} \cdot [(h_1 - h_8) + (h_3 - h_2)] \quad (10)$$

When the system operates without reheat, stream two is fed directly to the HTR, and the secondary turbine (T2) does not operate; the heat of thermal source is expressed by Eq. (11).

$$\dot{Q}_{tm} = \dot{m}_{CO2} \cdot (h_1 - h_8) \quad (11)$$

The general entropy balance was used to quantify the entropy generated in the system ($\dot{s}_{gen.i}$), as it is shown in Eq. (12).

$$\dot{s}_{gen.i} = \sum \dot{m}_{out} + s_{out} - \sum \dot{m}_{in} \cdot s_{in} - \sum \frac{\dot{Q}}{T} \quad (12)$$

The rate of exergy destruction for each component can also be determined using the exergy balance expressed by mean of Eq. (13).

$$\dot{E}D_{des} = \dot{E}D_{Q_i} - \dot{E}D_{W_i} + \sum \dot{m}_{in} \cdot e_{in} - \sum \dot{m}_{out} \cdot e_{out} \quad (13)$$

where $\dot{E}D_{Q_i}$ is the rate of exergy destroyed by heat transfer and $\dot{E}D_{W_i}$ is the rate of exergy destroyed by power.

The exergy destroyed by the heat transfer is given by Eq. (14).

$$\dot{E}Dx_{Q_i} = Q_i \cdot \left(1 - \frac{T_0}{T_s}\right) \quad (14)$$

where the heat transfer of the component Q_i is evaluated and the difference between the room temperature T_0 and the temperature at which heat is rejected from the system T_s.

The exergy of the working fluid found in the system is determined by Eq. (15).

$$e_i = h_i + h_0 + T_0 \cdot s_0 - T_0 \cdot s_i \quad (15)$$

The specific fuel consumption of the S-CO_2-SORC Brayton system ($BSFC_{Brayton-ORC}$) is calculated by Eq. (16).

$$BSFC_{Brayton-ORC} = \frac{\dot{m}_{fuel}}{\dot{W}_{net,ORC} + \dot{W}_{net,Brayton}} \quad (16)$$

The specific fuel consumption of the S-CO_2 Brayton cycle ($BSFC_{Brayton}$) is determined by Eq. (17).

$$BSFC_{Brayton} = \frac{\dot{m}_{fuel}}{\dot{W}_{net,Brayton}} \quad (17)$$

The latter shows a decrease when compared with the specific fuel consumption of the combined system Brayton S-CO_2-SORC is defined by Eq. (18).

$$\Delta BSFC = \frac{\left|BSFC_{Brayton-ORC} - BSFC_{Brayton}\right|}{BSFC_{Brayton}} \cdot 100 \quad (18)$$

It became necessary to calculate the thermal efficiency and the overall exergetic efficiency to determine and evaluate the performance of each of the components in the combined cycle. It was done to perform the thermodynamic analysis of the Brayton-ORC configuration.

2.4. Heat exchanger modeling: evaporator, condenser, heat recovery, and HTR

The heat transfer region (A_{ht}) for the system heat exchangers: plate and shell heat exchanger (HE1), evaporator (HE2), heat recovery (RC), and condenser (HE3), was obtained from the energy balance. It considers the heat transfer rate between the hot and cold streams (Girgin and Ezgi, 2017). For the evaporator (HE2) and condenser (HE3) the total heat transfer area is calculated as the sum of all transfer areas in each zone. The evaporator (HE2) is divided into three zones: preheating, evaporation, and overheating; the condenser is divided into two zone: cooling zone, and condensing zone. The working fluids exists in a single phase in the heat recovery (RC). The thermal oil and the cooling water are considered as a single phase. This method was based on the calculation the Number of Transfer Units ($\varepsilon - NTU$) and the Log-Mean Temperature Difference (LMDT), according to Eq. (19).

$$A_{ht} = \frac{1}{U_o} \cdot \frac{\dot{Q}}{\Delta T} \quad (19)$$

where $\dot{Q}$ is the rate of heat transfer expressed in kW, U_o is the overall heat transfer coefficient expressed in kW/m^2 K and ΔT is determined by Eq. (20).

$$\Delta T = \alpha \cdot \Delta T_{ml} \quad (20)$$

where ΔT_{ml} is the logarithmic mean temperature difference between the cold and hot fluid, and α is the correction factor. For the evaporator (HE2), condenser (HE3), and heat recovery (RC), α is equal to one. For the plate and shell heat exchanger (HE1), the ΔT_{ml} and α are determined by mean of Eqs. (21) and (22), respectively.

$$\Delta T_{ml} = \frac{\Delta T_1 - \Delta T_2}{ln\left(\frac{\Delta T_1}{\Delta T_2}\right)} \quad (21)$$

$$\alpha = \frac{\frac{\sqrt{P^2+1}}{P-1} \cdot [\ln(1-R) - \ln(1-P \cdot R)]}{ln\frac{2-R\cdot\left(P+1-\sqrt{P^2+1}\right)}{2-R\cdot\left(P+1+\sqrt{P^2+1}\right)}} \quad (22)$$

where ΔT_1 and ΔT_2 are the temperature difference of the fluid at the inlet and the outlet, respectively. P corresponds to the effectiveness coefficient, and R es the heat power ratio calculated by Eqs. (23) and (24).

$$R = \frac{T_{1AT} - T_{3AT}}{T_5 - T_6} \quad (23)$$

$$R = \frac{T_5 - T_6}{T_{1AT} - T_{3AT}} \quad (24)$$

Table 3
Model to determine the base cost of equipment.

Component	Base case (C_B^0)	
HE1, HE2, HE3, RC, HTR, RH,	$\log C_B^0 = K_1 + K_2 \cdot \log A_{ht} + K_3 \cdot (\log A_{ht})^2$	(34)
T1, T2, T3 C1, P1, P2	$\log C_B^0 = K_1 + K_2 \cdot \log \dot{W} + K_3 \cdot (\log \dot{W})^2$	(35)

For the shell and tube heat exchanger (HE1), the overall heat transfer coefficient (U_o) is determined by mean of Eq. (25), considering the external diameter (D_{ext}) and the internal diameter of the tube (D_{int}) (Kücük et al., 2019).

$$U_o = \frac{1}{\frac{D_{ext}}{D_{int} \cdot h_t} + \frac{D_{ext}}{2k_t} \cdot \ln \frac{D_{ext}}{D_{int}} + \frac{1}{h_s}} \tag{25}$$

where h_s is the convection heat transfer coefficient of the shell expressed in kW/m^2 K, h_t is the convection heat transfer coefficient of the tube side expressed with the same units and k_t is the thermal conductivity expressed in kW/m K.

While that, for the evaporator (HE2), condenser (HE3), and the heat recovery (RC), the heat transfer coefficient is calculated considering the thermal resistance between the hot and cold fluid given by Eq. (26).

$$\frac{1}{U_o} = \frac{1}{h_c} + \Psi_w + \frac{1}{h_h} \tag{26}$$

where h_c and h_h are the heat transfer coefficients on the hot and cold sides, respectively, and Ψ_w is the resistance of the material of the wall.

For the single phase zone the heat transfer coefficient in the evaporator, condenser and heat recovery (RC) is calculated by Eq. (27) (Ayub, 2003).

$$Nu = \frac{h \cdot D_h}{k} = 0.78 \cdot R_e^{0.5} \cdot P_r^{1/3}, 10 < Re < 20,000 \tag{27}$$

where k is the thermal conductivity, h is the heat transfer coefficient, D_h is the hydraulic diameter, P_r is the Prandtl number, and R_e is the Reynolds number.

In the two-phase zone, the heat transfer coefficient in the evaporator is obtained by Eq. (28) (Huang et al., 2012).

$$Nu = \frac{h \cdot D_h}{k} = 0.00187 \cdot \left(\frac{q \cdot d_0}{k_f}\right)^{0.56} \cdot \left(\frac{d_0 \cdot h_{fg}}{\alpha_i^2}\right)^{0.31} \cdot P_r^{0.35} \tag{28}$$

where h_{fg} is the latent heat of evaporation (J kg^{-1}) q is the heat flux (W m^{-1}), d_0 in the bubble departure diameter (m), k_f is the liquid-phase thermal conductivity, and α_i is the thermal diffusivity (m^2 S^{-1}).

In the two-phase zone of the condenser, the two-phase heat transfer coefficient is calculated by means of Eqs. (29) and (30), respectively.

$$Nu = \frac{h \cdot D_h}{k} = 4.118 \cdot \left(Re_{eq}\right)^{0.4} \cdot P_{r,l}^{0.33} \tag{29}$$

$$Re_{eq} = G \cdot \left[1 - x_m + x_m \left(\frac{\rho_l}{\rho_v}\right)^{0.5}\right] \cdot \frac{D}{\mu_l} \tag{30}$$

where Re_{eq} is the Reynolds number for equivalent mass flow rate (G), $P_{r,l}$ is the Prandtl number of the phase liquid, x_m is the vapor quality, ρ_l and ρ_v are the densities in the liquid and vapor phase, respectively, and μ_l is the dynamic viscosity of the phase liquid.

Finally, the heat transfer area is calculated as the sum of the areas required for each phase for the evaporator and condenser. On the other hand, considering the printed circuit heat exchanger (HTR), the overall heat transfer coefficient (U_o) is determined by Eq. (31) (Nikitin et al., 2006).

$$U_o = \frac{1}{\frac{1}{h_h} + \frac{A_h \cdot \Delta t_w}{A_w \cdot k_t} + \frac{A_h}{A_c \cdot h_c}} \tag{31}$$

where h_h and h_c correspond to the local heat transfer convective coefficients, calculated by Eqs. (32) and (33) (Nikitin et al., 2006). While A_c and A_h corresponds to the cold and hot side area.

$$h_h = 2.52 \cdot Re^{0.68}, (2800 \leq Re \leq 5800) \tag{32}$$

$$h_c = 5.49 \cdot Re^{0.63}, (6200 \leq Re \leq 12100) \tag{33}$$

2.5. Thermo-economic model

The estimation of investment costs is carried out through the *Module Costing Technique* (MCT) (Turton et al., 2018). This technique is accepted as the best technique for determining the preliminary costs of a plant in the absence of information on exact component costs (Sánchez Villafana and Vargas Machuca Bueno, 2019; Mata-Torres et al., 2019). The method estimates the value of the component considering the direct costs (acquisition, installation materials, workforce) and associated indirect costs (freight, insurance, and taxes, extra charges for construction).

The estimated cost considers the capacity indicator of each of the components of the combination between the ORC cycle and the S-CO_2 Brayton cycle. This indicator corresponds to the heat transfer area corresponding to any of the following equipment, heat exchanger, evaporator, condenser, heat recovery, and reheater. For the turbines, compressors, and pumps, the capacity indicator corresponds to the power of the equipment, which is calculated with the energy balance. The organic working fluids of this research have a small cost compared to the cost of the other equipment that composes the system. For this reason, they are not considered for economic analysis (Song et al., 2020).

The base costs (C_B^0) of each unit are determined by the expressions in Table 3, considering the standard pressure conditions and the manufacturing materials. Eq. (34) is used to calculate the base cost of the heat exchangers and the reheater, where the area (A_{ht}) is expressed in m^2. Eq. (35) determines the base cost of the turbines, compressors, and pumps. The coefficients K_1, K_2, and K_3 depending on the type of equipment and its capacity. Their values are shown in Table 5.

Once the base cost of each component is determined, the Unit Module Cost is calculated (C_{MOD}) using Table 4. For the turbines, the C_{MOD} is obtained with the factor F_{MOD}. Fort he other equipment, the C_{MOD} is calculated using coefficients B_1 and B_2, which depend on the type of equipment, and the factors F_M (material factor) and F_P (pressure factor). F_P is obtained on the basis of the operating pressure of the equipment expressed in *bar*, using (37).

The coefficients B_1, B_2, B_3, C_1, C_2, C_3, F_M and F_{MOD} used in Eqs. (36), (37) and (38) are shown in Table 5. These are classified for each of the equipment used in the different configurations depending on their geometry and operation.

Once the cost of each equipment is known, the cost of the S-CO_2-ORC Brayton is determined with Eq. (39).

$$C_{ORC,Brayton,2001} = \sum C_{MOD,i} \tag{39}$$

where i corresponds to each of the system components (heat exchanger, turbine, pump, etc.). It is used Eq. (40) to update the cost of the system from a prior date to a future date.

$$C_{ORC,Brayton,2018} = \frac{CEPCI_{2018}}{CEPCI_{2001}} C_{ORC,Brayton,2001} \tag{40}$$

where $CEPCI_{2001} = 397$ and $CEPCI_{2018} = 648.17$ (Li et al., 2019).

Table 4
Model for calculating the cost of the equipment module.

Component	Equipment module cost (C_{MOD})	
HE1, HE2, HE3, HTR RH, C, P1, P2	$C_{MOD} = C_B^0 \cdot (B_1 + B_2 \cdot F_M \cdot F_P)$	(36)
	$\log_{10} F_P = c_1 + c_2 \cdot \log_{10} P + c_3 \cdot (\log_{10} P)^2$	(37)
T1, T2, T3	$C_{MOD} = C_B^0 \cdot F_{MOD}$	(38)

Table 5
Coefficients for economic analysis model (Turton et al., 2018).

Component	K_1	K_2	K_3	C_1	C_2	C_3	B_1	B_2	F_M	F_{MOD}
HE1, HE2, HE3, RH, HTR	4.325	−0.303	0.163	0.039	−1.113	0.082	1.63	1.66	2.7	–
C1	2.290	1.360	−0.103						–	3.8
T1, T2, T3	2.705	1.440	−0.178	–	–	–	–	–	–	3.5
P1, P2	3.389	0.053	0.153	−0.394	0.396	−0.002	1.89	1.35	1.6	–

The annual investment cost (C_{IA}) can be determined by Eq. (41).

$$C_{IA} = \frac{n\,(1+n)^t}{(1+n)^t - 1}\, C_{ORC,Brayton,2018} \tag{41}$$

Values of interest rate n in the range from 1% to 13% were considered with a lifetime (t) of 20 years.

Some indicators such as LCOE, SIC, and PBP were considered to evaluate the thermo-economic performance of the system, The Leveled Cost of Energy (LCOE) was calculated using Eq. (42), based on the annual investment cost (C_{IA}), operating and maintenance costs ($O\&M_n$), the accumulated value of the energy generated by this investment $\dot{W}_g$ and the annual operating hours (H_A).

$$LCOE = \frac{C_{IA} + O\&M_A}{\dot{W}_g \cdot H_A} \tag{42}$$

It was assumed that the annual operating and maintenance costs ($O\&M_A$) are 3% of the annual investment cost (C_{IA}). The number of hours of annual operation (H_A) was taken as 7446 h (Shengjun et al., 2011).

Moreover, the SIC represents the profitability of the system based on the total cost of the S-CO_2 – ORC Brayton system (C_{total}) and the net power (W_{net}), see Eq. (43).

$$SIC_{ORC} = \frac{C_{total}}{W_{net}} \tag{43}$$

Finally, the PBP is evaluated using Eq. (44). This indicator represents the profitability of the system, considering the time required for the return on initial investment or the acquisition of economic resources in the thermal generation project.

$$PBP = \frac{-\ln\left(1 - i \cdot \frac{C_{total}}{S_{annual}}\right)}{\ln(1+i)} \tag{44}$$

where S_{annual} is the annual profitability cash flow in the lifetime, and i is the discount rate.

2.6. Multi-objective optimization and decision making

Four different methods are commonly used for multi-objective optimization. The first method is without preferences, the second used is an apriori method, the third is a combined method and the last is a posteriori method. This last method is the one implemented when applying a multi-object optimization with the Pareto optimal solution.

This method allows to select an optimal solution after having generated multiple solutions. The advantage of Pareto's boundary optimization is that it allows to obtain a cooperative solution. A set of Pareto solutions is considered optimal if, by moving from one solution to another, the improvement in the result of an objective function means a decrease in the result in another function. When the objective is to minimize the results of the objectives, Eq. (45) is applied.

$$X^* \in X : \forall e \in X.\ where\ F_i(e) \geq F_i(X^*) \forall_i, VF_i(e) > F_i(X^*)\ for\ at\ least\ one\ i \tag{45}$$

Where F is the vector of the objective functions of the optimization, i is the index of the functions, X is the feasible function, e is the vector of the decision variable and X^* is the optimal solution. On the other hand, to find a set of solutions for Pareto optimization with the ability to improve at least one of the objectives without deteriorating any other objective, the Equation es applied (46).

$$\forall i \in \{1, \ldots, N\}, f_i(\vec{a}) \leq f_i(\vec{x}),\ and\ \exists\{j \ldots, N\} : f_j(\vec{x}) < f_j(\vec{x}) \tag{46}$$

The method used by the optimization is based on the comparison of decision vectors. In the case where vector $\vec{x}$ dominates vector $\vec{a}$ it shows that vector $f(\vec{x})$ is better than vector $f(\vec{a})$ for all cases. When a solution cannot be dominated by any other solution, it indicates that this is the ideal solution for the method.

Table 6
Lower and upper boundary of the decision variables.

Decision Variables	Lower bound	Upper bound	Unit
Turbine inlet temperature, TIT	600	850	°C
High-pressure, P_{High}	20	28	MPa
Evaporator pinch point, PPT	15	35	°C
Pressure ratio, P_r	10	35	%

Four decision variables were considered in this work: turbine inlet temperature (TIT), high-pressure (P_{High}), evaporator pinch point temperature (PPT) and pressure ratio (P_r). For each variable a search range (vector) was defined, which are shown in Table 6.

Three objective functions were selected: net power, exergy efficiency, and specific investment cost (SIC). Subsequently, two scenarios were created considering bi-objective optimization cases which were: net power-SIC; and exergetic efficiency-SIC. The objective of these study scenarios was to search values within the search space of the decision variables (Table 6) that maximize net power and exergy efficiency at the lowest economic cost (SIC). This search procedure was applied for each configuration.

In this study, the optimization problem was approached using Non-Dominated Sorting Genetic Algorithm (NGSA)-II in Matlab Optimization Toolbox. This technique is based on the theory of evolution which consists of six steps: population, selection, reproduction, mutation, crossover, and migration. The values used in each step are shown in Table 7.

An example of a bi-optimization problem is shown in Fig. 3 where it is observed the set of dominant and non-dominant solutions, together with the so-called ideal solution and the non-ideal

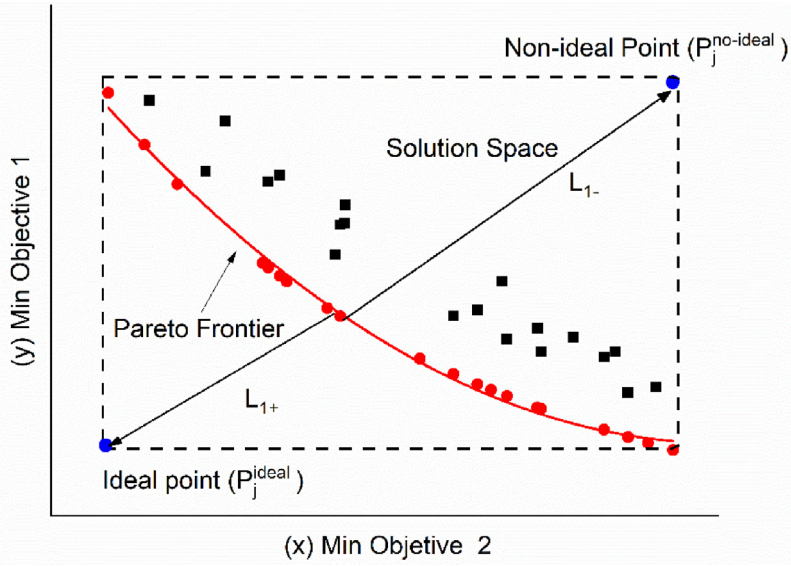

Fig. 3. Bi-objective optimization problem and decision-making approaches.

Table 7
Input parameters of optimization of NSGA II (Valencia et al., 2021).

Description	Value
Crossover fraction	0.80
Generation size	400
Selection process	Tournament
Migration fraction	0.2
Population size	50

solution. After obtaining the points within the search space (See Fig. 3) the solution must be determined. In this work the TOPSIS tool (Technique of Order Preference by Similarity to and Ideal Solution) was applied. Fig. 3 shows a typical case of minimization of two-objective functions. The red line indicates the Pareto optimal points; while the black dots indicate the Pareto non-optimal solution. Both optimal and non-optimal points are distributed within the solution space. The non-ideal solution ($P_j^{no-ideal}$) is the highest point within the search space; and the ideal solution P_j^{ideal} is the lowest point within the search space. Therefore, a solution must be found as close to the ideal and as far away from the non-ideal as possible (Jing et al., 2018).

To identify the solution, the Euclidean distance of each point was calculated according to Eqs. (47) and (48).

$$L_{i+} = \sqrt{\sum_{j=1}^{n}(P_{ij} - P_j^{ideal})^2} \tag{47}$$

$$L_{i-} = \sqrt{\sum_{j=1}^{n}(P_{ij} - P_j^{non-ideal})^2} \tag{48}$$

where i is the index of each solution of the Pareto frontier, and j is the index of the objective functions considered. The final selection is given by Eq. (49).

$$S_i = \frac{L_{i-}}{L_{i-} + L_{i+}} \tag{49}$$

2.7. Validation of modeling approach

Due to the fact that the literature results usually use supercritical recompression Brayton cycle, in this work it was decided to validate the models independently. In this way it was verified that both models are within the range as reported in the literature. For the validation of the RORC configuration, the results presented by El-Emam and Dincer (2013) and Zare (2015) were used. These works evaluated the performance of a regenerative organic Rankine cycle using geothermal source. The values used are presented in Table 8.

Table 8
Input data for the validation of the RORC layout.

η_{pum}	η_{tur}	T_{Geo} [°C]	$\dot{m}$ [kg/s]	T_{Cond}[°C]	T_{Pinch} [°C]	P_{Evap}[Bar]	Fluid
0.95	0.89	165	84.36	15	10	0,31	Isobutane

The results of the model comparison are shown in Table 9. The results show a good correlation in terms of thermal efficiency with errors between 0.7–0.62% in contrast to the results obtained by R. S. El-Emam et al. and V. Zare. A similar case was found for the exergetic efficiency with percentage errors between 0.18–0.35%. This shows that the model does not present significant differences and can be used correctly.

The energy model of the supercritical simple Brayton cycle was validated with the model proposed by Padilla et al. (2015). Table 10 shows the input data for validation.

The results shown in Fig. 4 show good correlation with the model proposed by Padilla et al. (2015). According to previous studies, the incorporation of Rankine cycles integrated to Brayton cycle configurations offers a significant increase in energy and exegetic efficiency, depending on the type of the Brayton configuration used: simple, recompression, intercooling. In that sense, Besarati and Yogi Goswami (2013) reported an increase in the overall thermal efficiency between 3%–7% of a recompression Brayton cycle coupled to an ORC cycle. Similar result was found by Akbari and Mahmoudi (2014) who evaluated the performance of a recompression Brayton cycle integrated to a simple organic Rankine cycle (SORC) . The results revealed that the integration of the organic Rankine cycle increases the overall exergy efficiency of the system by 11.7%. Based on the above, it is evident that the incorporation of Rankine cycle increases the energy and exergy efficiency of the Brayton cycle. This shows that the results shown in this work are correctly aligned with what is reported in the literature.

Table 9
Comparison results of the RORC model.

Parameters	Proposed Model	El-Emam et al. (El-Emam and Dincer, 2013)	V. Zare (Zare, 2015)	Error [%]
η_I(%)	16.25	16.37	16.15	0.7–0.62
η_{II}(%)	48.71	48.80	48.54	0.10–0.35

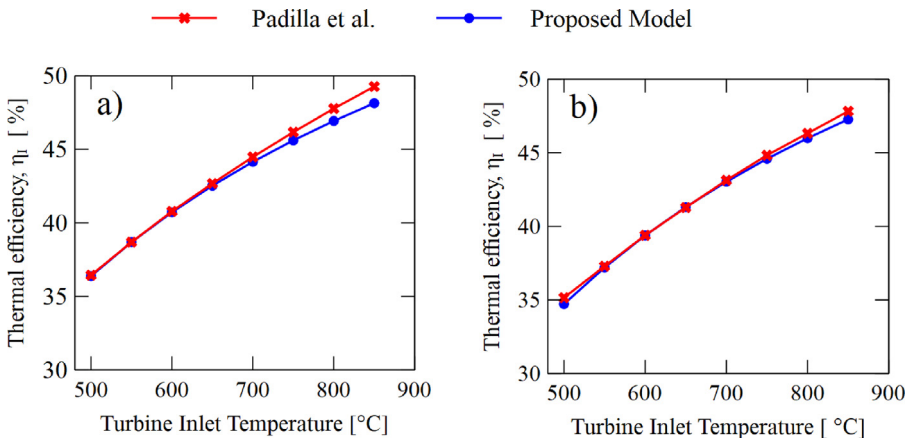

Fig. 4. Validation of the proposed model with Padilla et al.: (a) S-CO_2 Brayton cycle with reheat; (b) S-CO_2 Brayton cycle without reheat.

Table 10
Input parameters used in the validation of the supercritical simple Brayton cycle.

Parameters	Value
Compressor efficiency	89%
Turbine efficiency	93%
Turbine inlet temperature	550–800 °C
Turbine inlet pressure	25 MPa
Heat exchanger effectiveness	95%
Pressure drop in heat exchangers	0.0 kPa

3. Results and discussion

For the development of this study, the performance of the Brayton S-CO_2-SORC and Brayton S-CO_2-RORC configurations were analyzed considering the base conditions observed in Table 11.

The behavior of the energy, exergetic and economic indicators was studied for the S-CO_2-SORC Brayton cycle and the S-CO_2-RORC Brayton cycle systems with each of the working fluids (toluene, acetone, and cyclohexane) are shown in Table 12.

Table 12 shows that the system S-CO_2-RORC has a better performance than the S-CO_2-SORC system. Therefore, the addition of the heat recovery (RC) to the system causes an energy efficiency increase of about 13.91%, when the working fluid is cyclohexane, and 8.60% when the working fluid is toluene. These results agreed with some research conducted by Zhang et al. (2020). The two fluids provide high system efficiency due to their low enthalpy in the condenser along with the high operating temperatures. It increases the system efficiency of about 25.32% and 23.01% when using cyclohexane and toluene, respectively. Also, a higher system efficiency implies a reduction in fuel consumption of approximately 11.03% (cyclohexane) and 6.88% (toluene). It verifies that the selection is appropriate for the operating conditions used.

The energy performance indicators were calculated for each of the components of the S-CO_2-SORC and S-CO_2-RORC systems and for each of the selected working fluids considering the thermodynamic properties.

Table 13 shows that the components with the highest heat transfer rate for the two systems are HTR and R-HR, whose values correspond to 427.05 kW and 219.79 kW, respectively. Also, it can be observed that HE1 is the component with the highest exergy destruction rate for both, the S-CO_2-SORC system and the S-CO_2-RORC system. Therefore, this component has the highest contribution to the total exergy destroyed, as seen in Fig. 5. Its highest values are 23.14% (S-CO_2-SORC) and 21.01% (S-CO_2-RORC) when the fluid is toluene. It indicates that this component has a heat transfer area of 88.70 m^2 representing the highest value along with the R-HR.

Table 11
System parameters used in the Brayton S-CO_2-SORC and Brayton S-CO_2-RORC.

Configuration	Parameter	Value	Unit	Reference
SORC/RORC	Isentropic efficiency turbine	80	%	Valencia et al. (2019)
	Isentropic efficiency pumps	75	%	Valencia et al. (2019)
	Cooling water temperature (T1A)	50	°C	Valencia et al. (2019)
	Pinch point condenser (HE3)	15	°C	Valencia et al. (2019)
	Pressure ratio pump - 1 (P1)	2.5		Valencia et al. (2019)
	Pinch point evaporator (HE2)	15–35	°C	Valencia et al. (2019)
	Pressure ratio pump - 2 (P2)	30		Valencia et al. (2019)
Brayton	Turbine inlet temperature, TIT	550–750	°C	Padilla et al. (2015)
	Brayton cycle - High Pressure, P_{High}	20–25	MPa	Padilla et al. (2015)
	Efficiency - Brayton Turbines	93	%	Padilla et al. (2015)
	Efficiency compressor	89	%	Padilla et al. (2015)
	Effectiveness of HTR	95	%	Padilla et al. (2015)
	Pinch point minimum temperature	5	°C	Padilla et al. (2015)

Table 12
Energetic and economic indicator for the S-CO_2-SORC layout.

Indicators	S-CO_2-SORC			S-CO_2-RORC		
	Toluene	Acetone	Cyclohexane	Toluene	Acetone	Cyclohexane
$\dot{W}_{net,ORC}$ [kW]	26.11	29.74	26.41	33.57	32.78	36.02
$\dot{W}_{net,sCO_2-ORC}$ [kW]	137.64	141.27	137.94	144.30	144.30	147.55
$\eta_{I,ORC}$ [%]	16.67	18.99	16.86	21.43	20.93	23.00
η_{I,sCO_2-ORC} [%]	50.99	52.33	51.10	53.75	53.46	54.66
$\Delta\eta_{th}$ [%]	23.41	26.67	23.68	30.10	29.29	22.30
$BSFC_{sCO_2-ORC}$ [g/kWh]	147.07	143.29	146.75	139.51	140.28	137.19
$\Delta BSFC$ [%]	18.98	21.06	19.15	23.14	22.72	24.42
LCOE [USD/kWh]	0.19	0.18	0.19	0.19	0.20	0.19
SIC [USD/ kWh]	1930.43	1906.85	1932.30	1987.49	2002.37	1982.87
PBP [Years]	8.23	8.13	8.24	8.47	8.54	8.46

Table 13
Indicators of the total heat transfer, the area of the components, and the destroyed exergy for the proposed configurations.

Component	Indicator	S-CO_2 -SORC			S-CO_2 -RORC		
		Cyclohexane	Toluene	Acetone	Cyclohexane	Toluene	Acetone
ITC1	$\dot{Q}$ [kW]	143.07	143.07	143.07	143.07	143.07	143.07
	A_k [m^2]	88.70	88.70	88.70	88.70	88.70	88.70
	$\dot{E}x_D$ [kW]	10.29	10.85	9.34	4.11	9.53	9.18
ITC2	$\dot{Q}$ [kW]	141.67	141.67	141.67	141.67	141.67	141.67
	A_k [m^2]	15.62	14.71	14.62	16.84	15.01	14.74
	$\dot{E}x_D$ [kW]	5.17	6.40	5.24	3.95	5.97	5.04
ITC3	$\dot{Q}$ [kW]	120.39	121.31	118.92	116.97	119.40	118.60
	A_k [m^2]	8.91	7.77	6.05	6.55	5.54	5.27
	$\dot{E}x_D$ [kW]	6.28	5.66	5.11	5.03	5.13	5.11
RHR	$\dot{Q}$ [kW]	219.70	219.70	219.70	219.70	219.70	219.70
	A_k [m^2]	89.12	89.12	89.12	89.12	89.12	89.12
	$\dot{E}x_D$ [kW]	6.07	6.07	6.07	6.07	6.07	6.07
HTR	$\dot{Q}$ [kW]	427.05	427.05	427.05	427.05	427.05	427.05
	A_k [m^2]	15.66	15.66	15.66	15.66	15.66	15.66
	$\dot{E}x_D$ [kW]	4.69	4.69	4.69	4.69	4.69	4.69
REC	$\dot{Q}$ [kW]				22.73	13.23	2.02
	A_k [m^2]				34.52	33.07	36.28
	$\dot{E}x_D$ [kW]				0.73	0.33	0.01
T1	$\dot{W}$ [kW]	156.82	156.82	156.82	156.82	156.82	156.82
	$\dot{E}x_D$ [kW]	3.96	3.96	3.96	3.96	3.96	3.96
T2	$\dot{W}$ [kW]	21.70	20.50	23.56	25.18	22.42	23.90
	$\dot{E}x_D$ [kW]	4.26	4.20	5.25	4.94	4.60	5.33
T3	$\dot{W}$ [kW]	75.88	75.88	75.88	75.88	75.88	75.88
	$\dot{E}x_D$ [kW]	4.91	4.91	4.91	4.91	4.91	4.91
C1	$\dot{W}$ [kW]	0.14	0.14	0.14	0.14	0.14	0.14
	$\dot{E}x_D$ [kW]	0.13	0.13	0.12	0.12	0.12	0.12
P1	$\dot{W}$ [kW]	0.41	0.14	0.81	0.48	0.15	0.82
	$\dot{E}x_D$ [kW]	0.09	0.03	0.18	0.11	0.03	0.18
P2	$\dot{W}$ [kW]	143.07	143.07	143.07	143.07	143.07	143.07
	$\dot{E}x_D$ [kW]	88.70	88.70	88.70	88.70	88.70	88.70

3.1. Sensitivity analysis: energy and exergy performance indicators

The variability of the S-CO_2-RORC Brayton configuration performance indicators for each of the working fluids is shown in Fig. 6. It considers the influence of some parameters such as input temperature (TIT), high pressure (P_{High}), evaporator pinch point temperature (PPT), and pressure ratio (P_r).

The behavior of the system net power ($W_{NETBRAYTON-RORC}$) for the different selected fluids, and the rest of the parameters is presented in Fig. 6a to 6d. It can be seen in Fig. 6a that an increase in the inlet temperature of the turbine in the range from 550 to 750 °C causes an increase in the net system power about 22.89% (toluene), 29.50% (acetone) and 23.54% (cyclohexane). Fig. 6b showed a similar trend when the high pressure was increased from 20 to 28 MPa, and the pinch point (Fig. 6c) increased from 15 to 35 °C. It achieves a power increase of 2.23% and 3.08% (toluene), 2.23% and 9.37% (acetone) and 2.08% and 3.56% (cyclohexane), respectively. When the pressure ratio (P_r) is increased from 20 to 40 MPa (acetone and cyclohexane) and 20 to 100 MPa (toluene), it is observed that the net power increases as well about 7.70% (toluene), 3.62% (acetone) and 6.11% (cyclohexane). The result shows that it is necessary to select the cyclohexane as the working fluid to enhance this indicator. However, the increase in percentages is not as high as compared to the other two fluids. The range of results provides better performance in terms of the net power of the system.

Figs. 6e to 6h show the behavior of the thermal efficiency of the system ($\eta_{THBRAYTON-RORC}$). Fig. 6e shows that an increase in the turbine input temperature increases the thermal efficiency of the system by about 12.78% (toluene), 14.65% (acetone), and 12.70% (cyclohexane). In Fig. 6h, when the pressure ratio is increased, it is obtained an increase in the turbine input temperature, about 7.70% (toluene), 3.62% (acetone), and 6.11% (cyclohexane) is obtained.

On the other hand, a decrease in the thermal efficiency of the system is obtained ($\eta_{THBRAYTON-RORC}$) when the high pressure and pinch point are increased. When the organic fluid is toluene, and the high pressure and pinch point temperature are raised, the thermal efficiency of the system decreases by 1.24% and 0.73%, respectively. These results are 2.30% and 3.62% when working

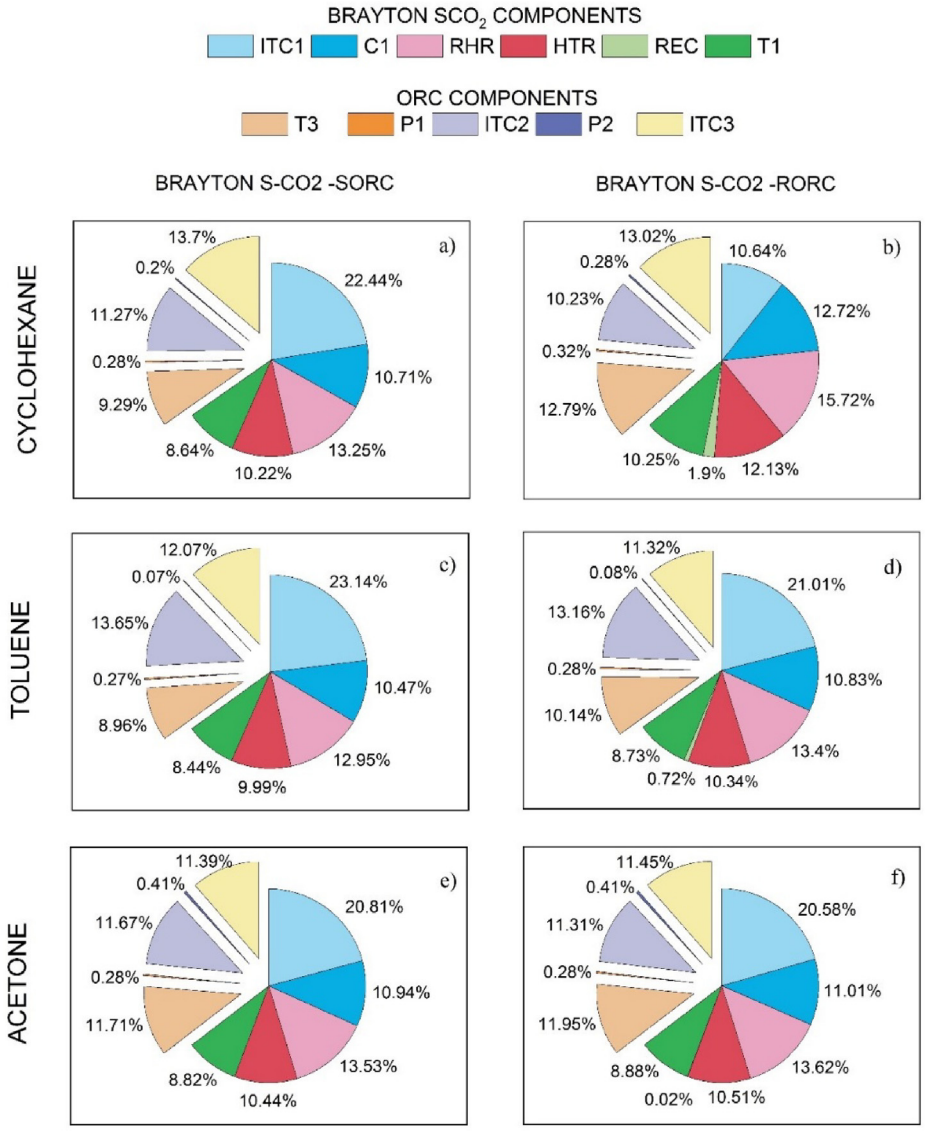

Fig. 5. Exergy destruction in the S-CO_2-SORC and Brayton S-CO_2-RORC components using different working fluids.

with acetone. When working with cyclohexane, the results are 1.38% and 0.89%.

The results for the delta efficiency of the system ($\Delta\eta$) are shown from Figs. 6i to 6l. Figs. 6i, 6j, and 6l show that an increase in the values of the inlet temperature, high pressure in the turbine, and pressure ratio leads to a decrease in the delta efficiency of the system ($\Delta\eta$). When the inlet temperature is increased, the results are 17.38% (toluene), 9.63% (acetone), and 16.89% (cyclohexane). When it is increased the high pressure, the results are 8.36% (toluene), 8.36% (acetone) *y* 8.50% (cyclohexane); 3.08% (toluene), 9.37% (acetone), 3.56% (cyclohexane), with respect to the pinch point (Fig. 6k). As for the pressure ratio, as shown in Fig. 6l, there is an increment in delta efficiency of 28.05% (toluene), 15.94% (acetone) and 25.03% (cyclohexane).

Figs. 6a to 6d show the specific fuel consumption ($\Delta BSFC$). It can be seen that fuel consumption decreases when increasing the inlet temperature in the turbine, the high pressure, and the pinch point temperature. Considering the inlet temperature in the turbine, see Fig. 6a, it is obtained a decrease in the $\Delta BSFC$ about 13.63% (toluene), 7.54% (acetone) and 13.03% (cyclohexane). When increasing the high pressure (Fig. 6b), it is obtained a decrease in the $\Delta BSFC$ about 6.49% (toluene), 6.49% (acetone) and 6.49% (cyclohexane). In the case of the pinch point (Fig. 6c), the decrease of the $\Delta BSFC$ is about 2.37% (toluene), 7.24% (acetone), and 2.69% (cyclohexane). Finally, when increasing the pressure ratio, Fig. 6d, it is obtained that the $\Delta BSFC$ increases about 22.05% (toluene), 12.78% (acetone), and 20% (cyclohexane).

The exergetic efficiency of the S-CO_2-SORC Brayton cycle, shown in Fig. 6e, indicates that an increase in the inlet temperature of the turbine improves this indicator about 1.12% (toluene), 3.23% (acetone), and 1.02% (cyclohexane). Fig. 6h shows the results considering the pressure ratio. An increase in this ratio causes an increase in exergetic efficiency of about 7.70% (toluene), 3.62% (acetone), and 6.11% (cyclohexane). On the other hand, when decreasing the high pressure (Fig. 6f) and the pinch point (Fig. 6 g), it is obtained an increase in the exergetic efficiency about 0.53% and 0.73% (toluene), 0.53% and 2.30% (acetone), 0.68% and 0.89% (cyclohexane), respectively.

Considering the overall energy efficiency of the system ($\eta_{WHROVERALL}$), shown from Fig. 6i to 6l, the combined cycle achieves better performance when the inlet temperature in the turbine is 750 °C (Fig. 6i). The results in the increase of total energy efficiency are 11.46%, 19.06%, 11.99%, when the working fluids are toluene, acetone, and cyclohexane, respectively. Similar behavior

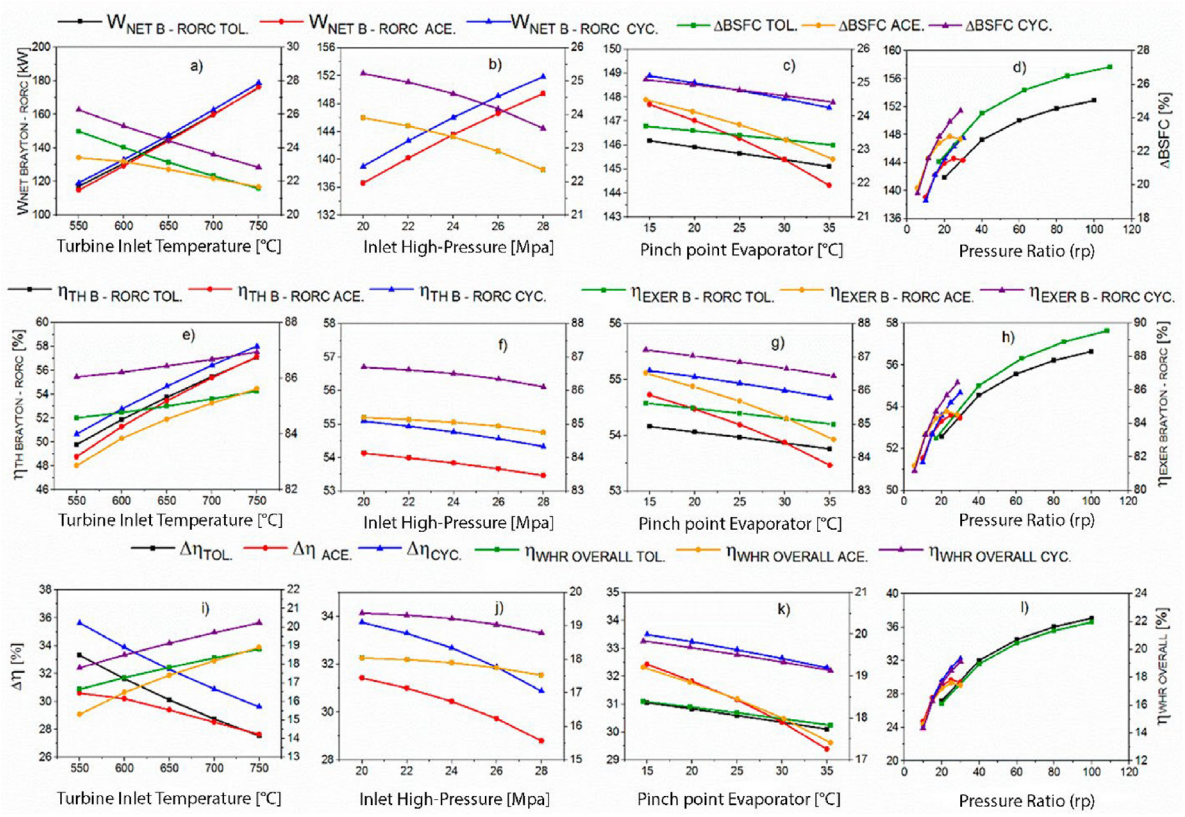

Fig. 6. Performance of the S-CO2-RORC Brayton configuration as a function of: (a–i) turbine inlet temperature (TIT); (b–j) Inlet High-Pressure (P_{high}); (c–k) pinch point evaporator (AP); (d–l) pressure ratio pump -2.

is obtained when the pressure ratio is increased (Fig. 6l). The results show an increase in the overall energy efficiency of about 28.04% (toluene), 15.94% (acetone), and 25.03% (cyclohexane). The behavior is opposite when increasing the high pressure (Fig. 6j). Hence, when the high-pressure Increase, it is obtained a decreased of about 2.88% (toluene), 2.88% (Acetone), and 3.02% (Cyclohexane). In the case of the Pinch point (Fig. 6k), the best results are obtained at a temperature of 15 °C. These results are 3.08% (toluene), 9.37 (acetone) and 9.37% (cyclohexane).

It can be demonstrated that the supercritical Brayton cycle integrated with the RORC cycle presents higher energetic and exergetic indicators when comparing the previous results with those obtained from the S-CO_2-SORC Brayton configuration. The result is much better when cyclohexane is selected as a working fluid. An increase of 7% in thermal efficiency can be achieved, indicating its high capacity to be used for industrial applications.

3.2. Sensitivity analysis: HTR effectiveness

Heat recovery is added to the system to optimize the performance of the Brayton S-CO_2-SORC configuration. Figs. 7a and 7b shows the thermal efficiency behavior for S-CO_2 Brayton configurations with heat recovery and with no heat recovery. Different fluids were analyzed in the system with heat recovery. The results revealed that the cyclohexane presented the best thermal efficiency (35.26%) and HTR effectiveness (70%). Another important variable analyzed was the influence of temperature on the effectiveness of this equipment. Figs. 7c and 7d shows that the higher the temperature the higher the effectiveness. The configuration without a heat recovery system can handle higher temperatures presenting a maximum operating temperature of 725 °C. It lets a better use of the fluid properties through the system and reach higher temperatures when it enters the turbine 1.

3.3. Sensitivity analysis: thermo-economic indicators

The economic performance assessment lets to analyze the behavior of the fluids that were selected for the operation of the two configurations studied. It identifies the fluid that presents the best economic performance, as shown in Fig. 8. The financial cost of fuel is one of the most influential variables in the operating costs of a system. Fig. 8a shows that the increase in the cost is directly proportional to the rise in the inlet temperature of the turbine. It increases by about 13% in the costs for a difference in temperature of 200 °C. The S-CO_2-SORC configuration shows a better fluid performance than the configuration that includes a heat recovery in the ORC coupling cycle.

The economic performance assessment lets to analyze the behavior of the fluids that were selected for the operation of the two configurations studied. It identifies the fluid that presents the best economic performance, as shown in Fig. 8. The financial cost of fuel is one of the most influential variables in the operating costs of a system. Fig. 8a shows that the increase in the cost is directly proportional to the rise in the inlet temperature of the turbine. It increases by about 13% in the costs for a difference in temperature of 200 °C. The S-CO_2-SORC configuration shows a better fluid performance than the configuration that includes a heat recovery in the ORC coupling cycle.

Figs. 8e to 8h show the behavior of the economic indicator (LCOE) as a function of the different variables used in the two configurations.

It indicates that the variables with the highest influence on this economic parameter are the TIT and the P_{High} of the turbine. Fig. 8e shows how the LCOE decreases with the increase of the system temperature. The LCOE has a significant decrease of 23% when the inlet temperature increases from 550 °C to 750 °C. It was optimized the performance of the two configurations for the

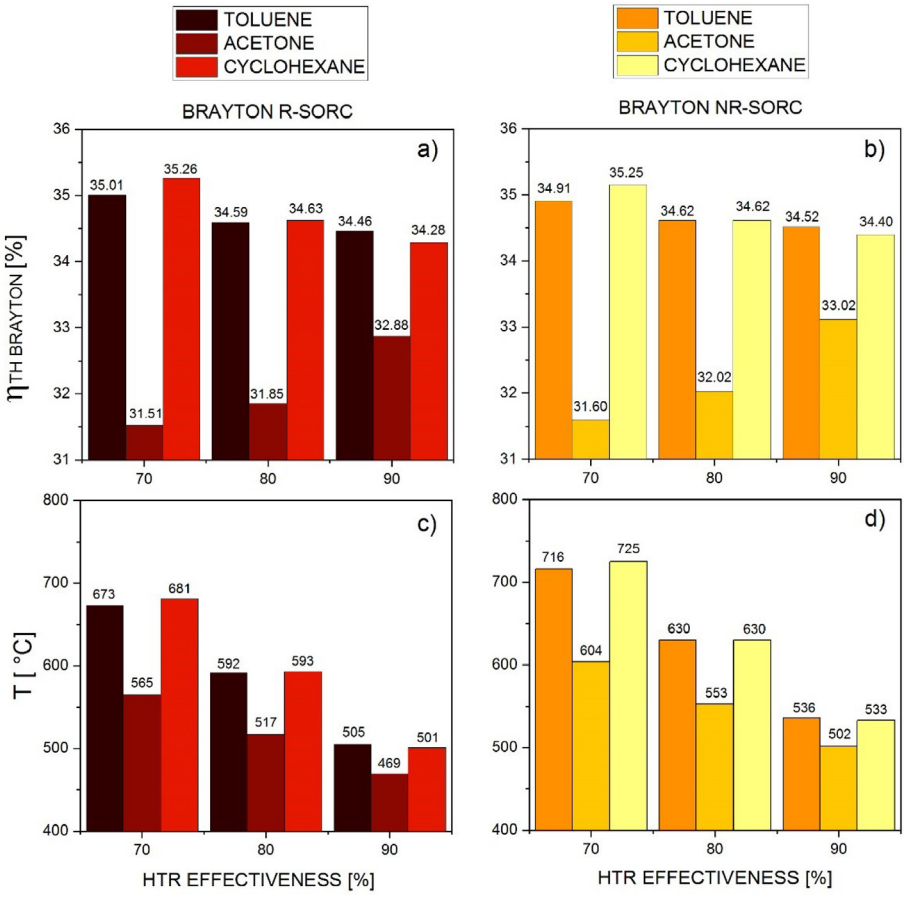

Fig. 7. HTR effectiveness for the three working fluids in the Brayton S-CO2-SORC with heat recovery (R) and without heat recovery (NR).

three working fluids used, considering the LCOE reference value (0.1652 USD/kWh).

Figs. 8i to 8l shows the SIC indicator. It determines the profitability of the system, considering the generated power. It can be seen that the results obtained are above the reference values (SIC Ref-1500 USD/kWh), with a difference of 12% when compared to the best results obtained. It was found that the increase in the operating temperature was the parameter that optimizes the profitability of the system.

On the other hand, the PBP is the economic indicator that determines the return time of the investment, as seen from Fig. 8m to 8p. It can be observed that the two configurations of the Brayton-ORC cycles with the working operating conditions, let to obtain the best results in the minimization of PBP when increasing the parameters TIT and P_{High}.

It can be seen in Fig. 8m that at a turbine inlet temperature of 750 °C, the PBP has an average of 7.5 years. Fig. 8p shows that it is obtained an average PBP value of 8.2 years when the P_{High} is 28 MPa. These results are below the reference value (PBP Ref-8.46 year). It helps to determine the parameters that result in the best performance of the mentioned configurations.

3.4. Multi-objective optimization

This section analyzes the results obtained from the multivariate thermo-economic optimization of each of the SORC and RORC configurations proposed in this study. The objective of this optimization is to find the optimal operating point of the System to obtain a better performance between investment cost and net power produced. To carry out the analysis, four input variables were proposed, which have the greatest impact on the behavior of the configurations, allowing us to find variable operating ranges in which an energetic efficiency of the system combined with the SORC of 79.40% is obtained, and in the case of the RORC configuration of 88.41%. Fig. 9 shows the operating ranges in which the decision variables of the system were evaluated. The characteristics of each configuration require a narrower range of operation of the components. In the case of the operating temperature for the two configurations, the operating limits are 600–850 °C as shown in Fig. 9a and 9b, where the optimal points for SORC (848.98 °C) and RORC (849.99 °C) were found, showing that the best operating conditions occur at higher temperatures due to the heat utilization in the systems.

Figs. 9c and 9d show the behavior of the system pressure for the SORC and RORC systems, allowing an analysis to be made of the fact that the data cloud in the RORC system (27.1 to 27.7 MPa) behaves close to the optimum operating point (27.66 MPa), while the SORC system shows greater variability in the data cloud, with the optimization behavior at the limits (20 to 28 MPa), but finding the optimum performance point at 27.25 MPa.

Figs. 9e and 9f show the data clouds of the system behavior for the decision variable PPT, allowing to analyze that this component is primordial to guarantee the heat removal from the systems to obtain the highest exergetic efficiency possible, showing that the SORC system requires an PPT of 31.97 °C with respect to the RORC that only requires a delta of 16.95 °C, determining that the SORC configuration requires a more robust equipment to be able to maintain the necessary operating conditions to reach the highest exergetic efficiency available of the system. The behavior of the P_r in the systems is presented in Fig. 9g and 9h, where the systems obtain an optimal pressure ratio point of 34.99

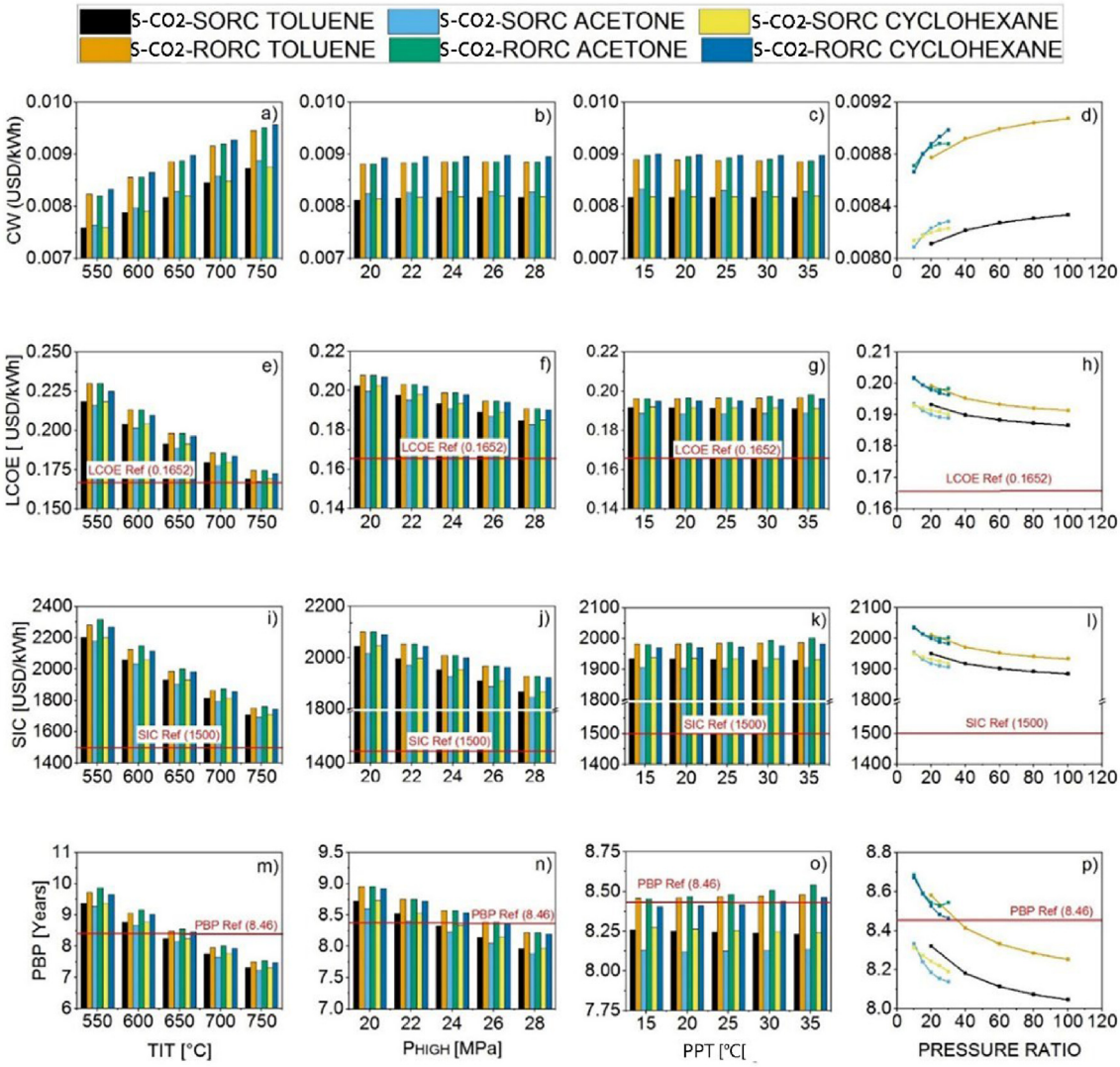

Fig. 8. Behavior of economic parameters for different working fluids in the S-CO_2-SORC and Brayton S-CO_2-RORC configurations.

MPa to achieve the highest exergetic efficiency that can be offered by the systems.

Multi-objective optimization was applied to the option that uses cyclohexane as working fluid. To achieve this, four objective functions were used. These functions were net power (W_{net}), exergetic efficiency (η_{exer}) and SIC, which were combined and presented in Fig. 8. The first proposed combination is optimization aiming at minimum SIC and maximum W_{net} (Fig. 8a–b), and the second is optimization by minimizing the ICS and increasing the exergetic efficiency. (Fig. 8 c–f) for the RORC and SORC system. In these Pareto diagrams 3 points of great relevance are highlighted. The first point (a) is the ideal solution reached by the optimization process. The second point (b) is the value of the base case of the study. This is the place of part of this work, and in it we see the power generated and the exergetic efficiency before the optimization. The last point (c) highlights the non-ideal solution achieved through the optimization process.

Fig. 10a shows the optimization by means of the Pareto frontier for the SIC and the net power in the RORC circuit. In it, it can be seen that the starting power value was 149 kWh and a value of 1982.87 for the SIC. The application of this optimization generated an increase in net power of approximately 40%, reaching a value of 213.23 kWh. Likewise, the SIC showed a decrease of approximately 24%, reaching a value of 1505.46. On the other hand, the behavior of the net power and the SIC analyzed for the SORC circuit is shown in Fig. 10b. It can be seen that the initial power value was 136.2 kWh and a SIC value of 1932.30. When the optimization was carried out, the power presented an increase of approximately 45% and a decrease of the SIC of approximately 31%.

The result of the optimization using as objective functions the exergetic efficiency and the SIC for the RORC cycle is presented in Fig. 10c. It is observed that the initial efficiency value is 84.1%. Said value increased up to 88.41%, representing an increase of 4.31%. This efficiency value corresponds to an SIC of 1454.77, which represents a decrease of approximately 36%. On the other hand, Fig. 10d shows the optimization of the SORC circuit with the exergetic efficiency and the SIC as object variables. For this case, the exergetic efficiency starts at 81.75% for the base values, and increases by approximately 4%, reaching a value of 85.85% in the optimal solution. To observe more clearly the behavior of the variables involved in the optimization, the basic design parameters for the RORC circuit will be presented in Table 13. Here we observe the values of the base case, the values of the decision variables for the optimization using the SIC and the exergetic efficiency as objective functions (option I), as well as the values of the decision variables for the optimization in which the SIC and the net power were taken as objective functions (option

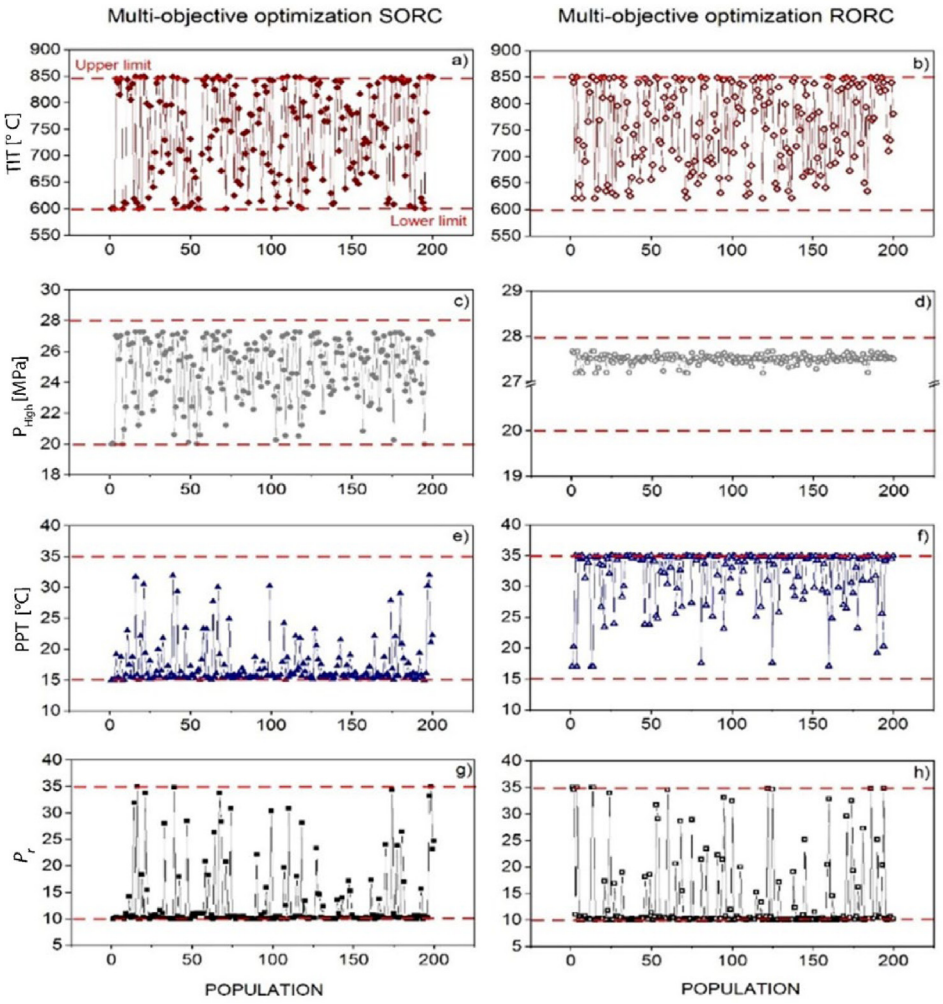

Fig. 9. Multi-objective optimization decision variables: (a–b) turbine inlet temperature (TIT), (c–d) high pressure, (e–f) Pinch point evaporator temperature (PPT), and (g–h) Pressure ratio (P_r).

Table 14
Optimized values for decision variables and objective functions in the RORC.

RORC Optimization				
Design parameters	Units	Base case	Option I	Option II
TIT	°C	650	838.31	849,99
P_{High}	kPa	25000	27260.93	27666.25
PPT	°C	30	24.6	16.95
P_r		35	32.12	34.99
Exergetic efficiency	%	84.1	88.41	87.82
Net power	kW	149	209.25	213.32
SIC	USD/kWh	1982.87	1460.56	1505.46

Table 15
Optimized values for decision variables and objective functions in the RORC.

SORC Optimization				
Design parameters	Units	Base case	Option I	Option II
TIT	°C	650	849.48	849.84
P_{High}	kPa	25000	27254.28	27282.46
PPT	°C	30	31.72	29.78
P_r		35	34.97	28.42
Exergetic efficiency	%	81.75	85.85	83.34
Net power	kW	136.2	196.15	198.73
SIC	USD/kWh	1932.30	1454.77	1467.57

II). In the same way, the values of the decision variables for the base case are presented in Table 14, together with the values of these variables the option I and the option II of the optimization (see Table 15).

4. Conclusions

In this research, it was assessed the energetic, exergetic and thermo-economic indicators of a Brayton S-CO_2 cycle integrated with an ORC (SORC or RORC) system to compare their performances considering three working fluids that are cyclohexane, toluene, and acetone.

The results showed that the implementation of heat recovery and the selection of cyclohexane as a working fluid caused an increase in the energy efficiency of about 13.91% as well as a reduction in the fuel consumption of approximately 11.03%. Also, with the analysis of the exergy destruction of each of the devices that integrate the system, it was found that the heat exchanger HE1 gives the highest contribution to the total exergy destroyed due to its high heat transfer area.

Regarding the thermo-economic indicators, the Brayton S-CO_2-SORC system had an excellent performance when working with Acetone, with an LCOE of 0.25 USD/kWh, a SIC of 2475.19 USD/kWh and a PBP of 10.55 years. Likewise, for the Brayton S-CO_2-RORC system, the best performance was found when working with cyclohexane, obtaining an LCOE of 0.169 USD/kWh, a SIC of 1691 USD/kWh and a PBP of 7.23 years.

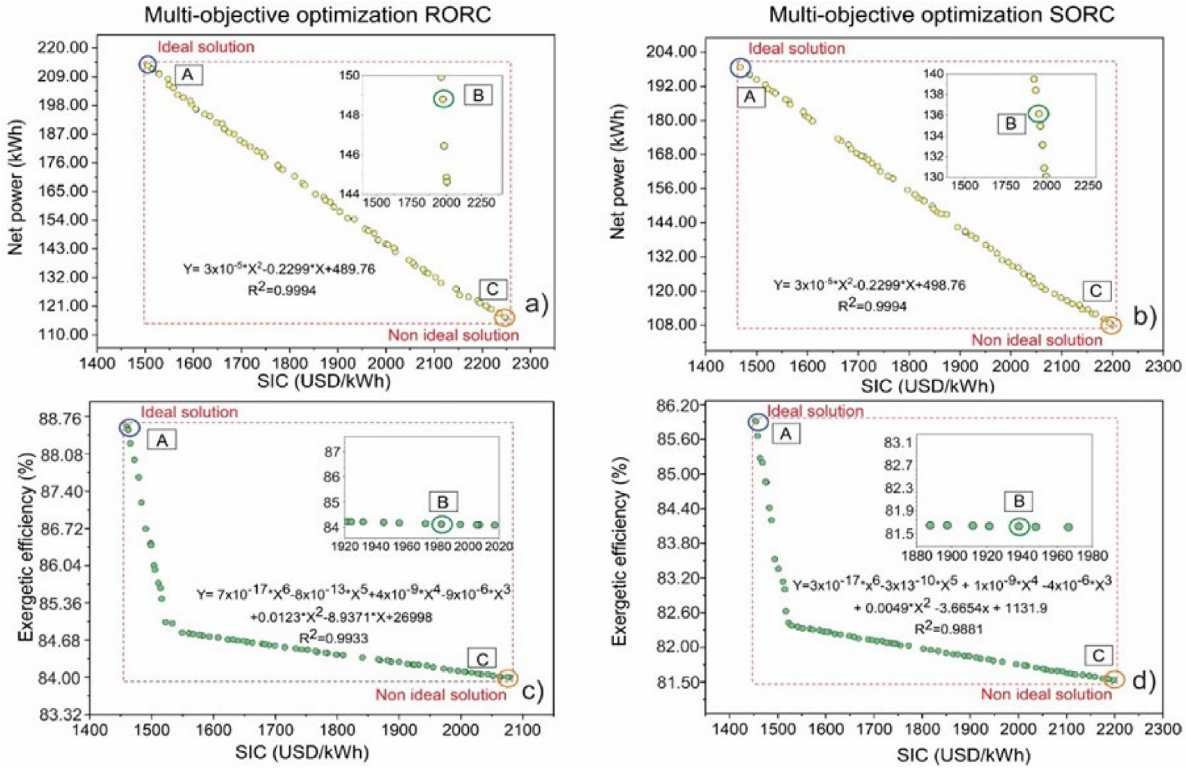

Fig. 10. Pareto frontier for objective functions (a–b) net power and SIC for RORC and SORC. (c–d) exegetic efficiency and SIC for RORC and SORC.

On the other hand, this work also allows us to conclude that, the increase in net power obtained through optimization using W_{net} and SIC as objective functions is very positive. With it, an increase of approximately 40% of the power for the RORC cycle and an increase of approximately 45% for the SORC cycle was achieved. A similar behavior was presented in the optimization using as objective functions the exergetic efficiency and the SIC, obtaining the optimal values for the efficiencies and presenting an increase in the powers. Achieving an increase in exergetic efficiency of approximately 4% for both cycles, and an increase in W_{net} of 40% and 44% for RORC and SORC respectively; it is possible to conclude that the optimization using as objective functions the exergetic efficiency and the SIC (option I) for the cycle RORC is the one that obtains the greater W_{net} maintaining a low SIC.

Nomenclature

SORC	Simple Organic Rankine cycle
BSFC	Brake specific fuel consumption
C	Cost ($) or compressor
HTR	High-temperature recuperator
HE	Heat exchanger
GWP	Global warming potential
RORC	Regenerative organic Rankine cycle
LCOE	Levelized cost of energy (USD/kWh)
ODP	Ozone depletion potential
P	Pump
PBP	Payback period (Year)
PPT	Pinch point temperature evaporator (°C)
RC	Heat recovery
SIC	Specific investment cost (USD/kWh)
TIT	Turbine inlet temperature (°C)
T	Turbine
Greek symbols	
A_p	Pinch point evaporator (°C)
D	Diameter
P_r	Pressure ratio (-)
$\dot{W}$	Work (kJ)
$\dot{Q}$	Heat transfer rate (kW)
C_{MOD}	Unit Module Cost ($)
η_I	Cycle thermal efficiency (%)
η_{II}	Cycle exergetic efficiency (%)
$\dot{m}$	Mass flow rate (kg/s)
$\dot{E}$	Exergy (kW)
e_i	Specific exergy (kJ/kg)
$\dot{E}D$	Exergy destroyed (kW)
A_{ht}	Heat transfer region (m^2)
U_o	Overall heat transfer coefficient (kW/m^2 K)
ΔT_{ml}	Logarithmic mean temperature difference
α	Correction factor (-)
h	Convection heat transfer coefficient (kW/m^2 K) or specific enthalpy (kJ/kg)
Re	Reynold number (-)
k_t	Thermal conductivity (kW/m K)
Subscripts	
Out	Outlet
In	Inlet
gen	Generated
HR	Heater
R-HR	Reheater
tm	Thermal source
t	Tube
tur	turbine
pum	pump
s	Shell
c	Cold
h	Hot
int	Internal
ext	External

Declaration of competing interest

The authors declare that they have no known competing financial interests or personal relationships that could have appeared to influence the work reported in this paper.

Data availability

No data was used for the research described in the article.

Acknowledgments

The authors want to acknowledge the support of the UNIVERSIDAD DEL ATLANTICO through the project ING564-CIS2022 "Análisis exergo-ambiental comparativo de dos sistemas híbridos de generación de energía basados en ciclos combinados brayton-orc" on the development of this research by providing access to their facility.

References

Abrosimov, K.A., Baccioli, A., Bischi, A., 2019. Techno-economic analysis of combined inverted Brayton – Organic Rankine cycle for high-temperature waste heat recovery. Energy Convers. Manag. X 3, 100014. http://dx.doi.org/10.1016/j.ecmx.2019.100014.

Akbari, A.D., Mahmoudi, S.M.S., 2014. Thermoeconomic analysis & optimization of the combined supercritical CO2 (carbon dioxide) recompression Brayton/organic Rankine cycle. Energy 78, 501–512. http://dx.doi.org/10.1016/j.energy.2014.10.037.

Ambiente, M.D.E., Territorial, D., 2008. Resolucion 909, Vol. 2008. p. 36.

Anon, 1998. Kyoto protocol to the United Nations framework convention on climate change United Nations.

Anon, 2017. NFPA 704: Standard System for the Identification of the Hazards of Materials for Emergency Response, Vol. 2017, 2017 ed. National Fire Protection Association, p. 2017.

Arbolino, R., Carlucci, F., Cirà, A., Ioppolo, G., Yigitcanlar, T., 2017. Efficiency of the EU regulation on greenhouse gas emissions in Italy: The hierarchical cluster analysis approach. Ecol. Indic. 81, 115–123. http://dx.doi.org/10.1016/j.ecolind.2017.05.053.

Ayub, Z.H., 2003. Plate heat exchanger literature survey and new heat transfer and pressure drop correlations for refrigerant evaporators. Heat Transf. Eng. 24, 3–16. http://dx.doi.org/10.1080/01457630304056.

Benato, A., Macor, A., Rossetti, A., 2017. Biogas engine emissions: Standards and on-site measurements. Energy Procedia 126, 398–405. http://dx.doi.org/10.1016/j.egypro.2017.08.278.

Besarati, S.M., Yogi Goswami, D., 2013. Analysis of advanced supercritical carbon dioxide power cycles with a bottoming cycle for concentrating solar power applications. J. Sol. Energy Eng. 136, http://dx.doi.org/10.1115/1.4025700.

Bouallaga, A., Davigny, A., Courtecuisse, V., Robyns, B., 2017. Methodology for technical and economic assessment of electric vehicles integration in distribution grid. Math. Comput. Simul. 131, 172–189. http://dx.doi.org/10.1016/j.matcom.2016.05.003.

Braimakis, K., Karellas, S., 2017. Integrated thermoeconomic optimization of standard and regenerative ORC for different heat source types and capacities. Energy 121, 570–598. http://dx.doi.org/10.1016/j.energy.2017.01.042.

Cao, Y., Li, P., Qiao, Z., Ren, S., Si, F., 2022. A concept of a supercritical CO2 Brayton and organic Rankine combined cycle for solar energy utilization with typical geothermal as auxiliary heat source: Thermodynamic analysis and optimization. Energy Rep. 8, 322–333. http://dx.doi.org/10.1016/j.egyr.2021.11.258.

Danieli, P., Rech, S., Lazzaretto, A., 2019. Supercritical CO2 and air Brayton–Joule versus ORC systems for heat recovery from glass furnaces: Performance and economic evaluation. Energy 168, 295–309. http://dx.doi.org/10.1016/j.energy.2018.11.089.

de Campos, G.B., Bringhenti, C., Traverso, A., Tomita, J.T., 2020. Thermoeconomic optimization of organic Rankine bottoming cycles for micro gas turbines. Appl. Therm. Eng. 164, 114477. http://dx.doi.org/10.1016/j.applthermaleng.2019.114477.

de Oliveira Neto, R., Sotomonte, C.A.R., Coronado, C.J.R., Nascimento, M.A.R., 2016. Technical and economic analyses of waste heat energy recovery from internal combustion engines by the Organic Rankine Cycle. Energy Convers. Manag. 129, 168–179. http://dx.doi.org/10.1016/j.enconman.2016.10.012.

Desai, N.B., Bandyopadhyay, S., 2009. Process integration of organic Rankine cycle. Energy 34, 1674–1686. http://dx.doi.org/10.1016/j.energy.2009.04.037.

Dudkiewicz, E., Szałański, P., 2020. Overview of exhaust gas heat recovery technologies for radiant heating systems in large halls. Therm. Sci. Eng. Prog. 18, 100522. http://dx.doi.org/10.1016/j.tsep.2020.100522.

El-Emam, R.S., Dincer, I., 2013. Exergy and exergoeconomic analyses and optimization of geothermal organic Rankine cycle. Appl. Therm. Eng. 59, 435–444. http://dx.doi.org/10.1016/j.applthermaleng.2013.06.005.

Girgin, I., Ezgi, C., 2017. Design and thermodynamic and thermoeconomic analysis of an organic Rankine cycle for naval surface ship applications. Energy Convers. Manag. 148, 623–634. http://dx.doi.org/10.1016/j.enconman.2017.06.033.

Grelet, V., Reiche, T., Lemort, V., Nadri, M., Dufour, P., 2016. Transient performance evaluation of waste heat recovery rankine cycle based system for heavy duty trucks. Appl. Energy 165, 878–892. http://dx.doi.org/10.1016/j.apenergy.2015.11.004.

Habibi, H., Zoghi, M., Chitsaz, A., Javaherdeh, K., Ayazpour, M., Bellos, E., 2020. Working fluid selection for regenerative supercritical Brayton cycle combined with bottoming ORC driven by molten salt solar power tower using energy–exergy analysis. Sustain. Energy Technol. Assess. 39, 100699. http://dx.doi.org/10.1016/j.seta.2020.100699.

Hou, S., Cao, S., Yu, L., Zhou, Y., Wu, Y., Zhang, F., 2018. Performance optimization of combined supercritical CO2 recompression cycle and regenerative organic Rankine cycle using zeotropic mixture fluid. Energy Convers. Manag. 166, 187–200. http://dx.doi.org/10.1016/j.enconman.2018.04.025.

Hou, Z., Wei, X., Ma, X., Meng, X., 2020. Exergoeconomic evaluation of waste heat power generation project employing organic rankine cycle. J. Clean. Prod. 246, 119064. http://dx.doi.org/10.1016/j.jclepro.2019.119064.

Huang, J., Sheer, T.J., Bailey-Mcewan, M., 2012. Heat transfer and pressure drop in plate heat exchanger refrigerant evaporators. Int. J. Refrig. 35, 325–335. http://dx.doi.org/10.1016/j.ijrefrig.2011.11.002.

Imran, M., Haglind, F., Asim, M., Zeb Alvi, J., 2018. Recent research trends in organic rankine cycle technology: A bibliometric approach. Renew. Sustain. Energy Rev. 81, 552–562. http://dx.doi.org/10.1016/j.rser.2017.08.028.

Invernizzi, C., Iora, P., Silva, P., 2007. Bottoming micro-rankine cycles for micro-gas turbines. Appl. Therm. Eng. 27, 100–110. http://dx.doi.org/10.1016/j.applthermaleng.2006.05.003.

Jaber, H., Khaled, M., Lemenand, T., Faraj, J., Bazzi, H., Ramadan, M., 2017. Effect of exhaust gases temperature on the performance of a hybrid heat recovery system. Energy Procedia 119, 775–782. http://dx.doi.org/10.1016/j.egypro.2017.07.110.

Jing, R., Zhu, X., Zhu, Z., Wang, W., Meng, C., Shah, N., Li, N., Zhao, Y., 2018. A multi-objective optimization and multi-criteria evaluation integrated framework for distributed energy system optimal planning. Energy Convers. Manag. 166, 445–462. http://dx.doi.org/10.1016/j.enconman.2018.04.054.

Khademi, M., Ahmadi, A., Dashti, R., Shirmohammadi, R., 2022. Thermoeconomic optimization of a solar-assisted supercritical CO2 Brayton cycle, organic Rankine cycle and multi-effect distillation system. Energy Rep. 8, 13494–13503. http://dx.doi.org/10.1016/j.egyr.2022.10.010.

Khaled, M., Murr, R., El Hage, H., Ramadan, M., Ramadan, H., Becherif, M., 2020. An iterative algorithm for simulating heat recovery from exhaust gas – Application on generators. Math. Comput. Simul. 167, 92–103. http://dx.doi.org/10.1016/j.matcom.2018.04.011.

Kim, Y.M., Kim, C.G., Favrat, D., 2012. Transcritical or supercritical CO2 cycles using both low- and high-temperature heat sources. Energy 43, 402–415. http://dx.doi.org/10.1016/j.energy.2012.03.076.

Kölsch, B., Radulovic, J., 2015. Utilisation of diesel engine waste heat by Organic Rankine Cycle. Appl. Therm. Eng. 78, 437–448. http://dx.doi.org/10.1016/j.applthermaleng.2015.01.004.

Kücük, H., Ünverdi, M., Senan Yılmaz, M., 2019. Experimental investigation of shell side heat transfer and pressure drop in a mini-channel shell and tube heat exchanger. Int. J. Heat Mass Transfer 143, 118493. http://dx.doi.org/10.1016/j.ijheatmasstransfer.2019.118493.

Li, T., Meng, N., Liu, J., Zhu, J., Kong, X., 2019. Thermodynamic and economic evaluation of the organic Rankine cycle (ORC) and two-stage series organic Rankine cycle (TSORC) for flue gas heat recovery. Energy Convers. Manag. 183, 816–829. http://dx.doi.org/10.1016/j.enconman.2018.12.094.

Liang, Y., Chen, J., Luo, X., Chen, J., Yang, Z., Chen, Y., 2020. Simultaneous optimization of combined supercritical CO2 Brayton cycle and organic Rankine cycle integrated with concentrated solar power system. J. Clean. Prod. 266, 121927. http://dx.doi.org/10.1016/j.jclepro.2020.121927.

Maizza, V., Maizza, A., 1996. Working fluids in non-steady flows for waste energy recovery systems. Appl. Therm. Eng. 16, 579–590. http://dx.doi.org/10.1016/1359-4311(95)00044-5.

Mata-Torres, C., Zurita, A., Cardemil, J.M., Escobar, R.A., 2019. Exergy cost and thermoeconomic analysis of a rankine cycle + multi-effect distillation plant considering time-varying conditions. Energy Convers. Manag. 192, 114–132. http://dx.doi.org/10.1016/j.enconman.2019.04.023.

Michos, C.N., Lion, S., Vlaskos, I., Taccani, R., 2017. Analysis of the backpressure effect of an Organic Rankine Cycle (ORC) evaporator on the exhaust line of a turbocharged heavy duty diesel power generator for marine applications. Energy Convers. Manag. 132, 347–360. http://dx.doi.org/10.1016/j.enconman.2016.11.025.

Mostafavi, S.A., Mahmoudi, M., 2018. Modeling and fabricating a prototype of a thermoelectric generator system of heat energy recovery from hot exhaust gases and evaluating the effects of important system parameters. Appl. Therm. Eng. 132, 624–636. http://dx.doi.org/10.1016/j.applthermaleng.2018.01.018.

Nami, H., Ertesvåg, I.S., Agromayor, R., Riboldi, L., Nord, L.O., 2018. Gas turbine exhaust gas heat recovery by organic Rankine cycles (ORC) for offshore combined heat and power applications - energy and exergy analysis. Energy http://dx.doi.org/10.1016/j.energy.2018.10.034.

Nikitin, K., Kato, Y., Ngo, L., 2006. Printed circuit heat exchanger thermal–hydraulic performance in supercritical CO2 experimental loop. Int. J. Refrig. 29, 807–814. http://dx.doi.org/10.1016/j.ijrefrig.2005.11.005.

Noaman, M., Saade, G., Morosuk, T., Tsatsaronis, G., 2019. Exergoeconomic analysis applied to supercritical CO2 power systems. Energy 183, 756–765. http://dx.doi.org/10.1016/j.energy.2019.06.161.

Novales, D., Erkoreka, A., De la Peña, V., Herrazti, B., 2019. Sensitivity analysis of supercritical CO2 power cycle energy and exergy efficiencies regarding cycle component efficiencies for concentrating solar power. Energy Convers. Manag. 182, 430–450. http://dx.doi.org/10.1016/j.enconman.2018.12.016.

Ochoa, G.V., Forero, J.D., Rojas, J.P., 2022. Thermoeconomic analysis of a combined supercritical CO2 reheating under different configurations of Organic Rankine cycle ORC as a bottoming cycle. Heliyon 8, e12230. http://dx.doi.org/10.1016/j.heliyon.2022.e12230.

Padilla, R.V., Soo Too, Y.C., Benito, R., Stein, W., 2015. Exergetic analysis of supercritical CO2 Brayton cycles integrated with solar central receivers. Appl. Energy 148, 348–365. http://dx.doi.org/10.1016/j.apenergy.2015.03.090.

Qiao, Z., Cao, Y., Li, P., Wang, X., Romero, C.E., Pan, L., 2020. Thermoeconomic analysis of a CO2 plume geothermal and supercritical CO2 Brayton combined cycle using solar energy as auxiliary heat source. J. Clean. Prod. 256, 120374. http://dx.doi.org/10.1016/j.jclepro.2020.120374.

Rahbar, K., Mahmoud, S., Al-Dadah, R.K., Moazami, N., Mirhadizadeh, S.A., 2017. Review of organic Rankine cycle for small-scale applications. Energy Convers. Manag. 134, 135–155. http://dx.doi.org/10.1016/j.enconman.2016.12.023.

Sánchez Villafana, E.D., Vargas Machuca Bueno, J.P., 2019. Thermoeconomic and environmental analysis and optimization of the supercritical CO2 cycle integration in a simple cycle power plant. Appl. Therm. Eng. 152, 1–12. http://dx.doi.org/10.1016/j.applthermaleng.2019.02.052.

Sara, H., Chalet, D., Cormerais, M., 2018. Different configurations of exhaust gas heat recovery in internal combustion engine: Evaluation on different driving cycles using numerical simulations. J. Therm. Sci. Eng. Appl. 10, 1–49. http://dx.doi.org/10.1115/1.4039304.

Sarkar, J., 2009. Second law analysis of supercritical CO2 recompression Brayton cycle. Energy 34, 1172–1178. http://dx.doi.org/10.1016/j.energy.2009.04.030.

Secretariat, O., 2000. United nations environment programme. Synth. Reports Sci. Environ. Eff. Technol. Econ. Assess. Panels Montr. Protoc.

Shengjun, Z., Huaixin, W., Tao, G., 2011. Performance comparison and parametric optimization of subcritical Organic Rankine Cycle (ORC) and transcritical power cycle system for low-temperature geothermal power generation. Appl. Energy 88, 2740–2754. http://dx.doi.org/10.1016/j.apenergy.2011.02.034.

Shi, L., Shu, G., Tian, H., Deng, S., 2018. A review of modified Organic Rankine cycles (ORCs) for internal combustion engine waste heat recovery (ICE-WHR). Renew. Sustain. Energy Rev. 92, 95–110. http://dx.doi.org/10.1016/j.rser.2018.04.023.

Song, J., Loo, P., Teo, J., Markides, C.N., 2020. Thermo-economic optimization of organic rankine cycle (ORC) systems for geothermal power generation: A comparative study of system configurations. Front. Energy Res. 8, 1–14. http://dx.doi.org/10.3389/fenrg.2020.00006.

Song, J., song Li, X., dong Ren, X., wei Gu, C., 2018. Performance analysis and parametric optimization of supercritical carbon dioxide (s-CO2) cycle with bottoming Organic Rankine Cycle (ORC). Energy 143, 406–416. http://dx.doi.org/10.1016/j.energy.2017.10.136.

Sukumaran, S., Sudhakar, K., 2018. Performance analysis of solar powered airport based on energy and exergy analysis. Energy 149, 1000–1009. http://dx.doi.org/10.1016/j.energy.2018.02.095.

Tartière, T., Astolfi, M., 2017. A world overview of the organic Rankine cycle market. Energy Procedia 129, 2–9.

Teng, L., Xuan, Y., 2019. Design of a composite receiver for solar-driven supercritical CO2 Brayton cycle. J. CO2 Util. 32, 290–298. http://dx.doi.org/10.1016/j.jcou.2019.05.006.

Thakar, R., Bhosle, S., Lahane, S., 2018. Design of heat exchanger for waste heat recovery from exhaust gas of diesel engine. Procedia Manuf. 20, 372–376. http://dx.doi.org/10.1016/j.promfg.2018.02.054.

Turton, R.A., Shaeiwitz, J.A., Bhattacharyya, Debangsu., Whiting, W.B., 2018. Analysis, Synthesis and Design of Chemical Processes, fifth ed. Boston Prentice Hall.

Uusitalo, A., Ameli, A., Turunen-Saaresti, T., 2019. Thermodynamic and turbomachinery design analysis of supercritical Brayton cycles for exhaust gas heat recovery. Energy 167, 60–79. http://dx.doi.org/10.1016/j.energy.2018.10.181.

Valencia, G., Fontalvo, A., Cárdenas, Y., Duarte, J., Isaza, C., 2019. Energy and exergy analysis of different exhaust waste heat recovery systems for natural gas engine based on ORC. Energies 12, http://dx.doi.org/10.3390/en12122378.

Valencia, G., Fontalvo, A., Duarte Forero, J., 2021. Optimization of waste heat recovery in internal combustion engine using a dual-loop organic rankine cycle: Thermo-economic and environmental footprint analysis. Appl. Therm. Eng. 182, 116109. http://dx.doi.org/10.1016/j.applthermaleng.2020.116109.

Valencia Ochoa, G., Duarte Forero, J., Rojas, J.P., 2020. A comparative energy and exergy optimization of a supercritical-CO2 Brayton cycle and Organic Rankine Cycle combined system using swarm intelligence algorithms. Heliyon 6, e04136. http://dx.doi.org/10.1016/j.heliyon.2020.e04136.

White, M.T., Oyewunmi, O.A., Chatzopoulou, M.A., Pantaleo, A.M., Haslam, A.J., Markides, C.N., 2018. Computer-aided working-fluid design, thermodynamic optimisation and thermoeconomic assessment of ORC systems for waste-heat recovery. Energy 161, 1181–1198. http://dx.doi.org/10.1016/j.energy.2018.07.098.

White, M.T., Oyewunmi, O.A., Haslam, A.J., Markides, C.N., 2017. Industrial waste-heat recovery through integrated computer-aided working-fluid and ORC system optimisation using SAFT-γ Mie. Energy Convers. Manag. 150, 851–869. http://dx.doi.org/10.1016/j.enconman.2017.03.048.

White, M.T., Sayma, A.I., 2019. Simultaneous cycle optimization and fluid selection for ORC systems accounting for the effect of the operating conditions on turbine efficiency. Front. Energy Res. 7, http://dx.doi.org/10.3389/fenrg.2019.00050.

Xia, X.X., Wang, Z.Q., Zhou, N.J., Hu, Y.H., Zhang, J.P., Chen, Y., 2020. Working fluid selection of dual-loop organic Rankine cycle using multi-objective optimization and improved grey relational analysis. Appl. Therm. Eng. 171, 115028. http://dx.doi.org/10.1016/j.applthermaleng.2020.115028.

Young, D., Gibson, S.C., Bandhauer, T.M., 2018. Working fluid selection and technoeconomic optimization of a turbocompression cooling system. J. Therm. Sci. Eng. Appl. 10, http://dx.doi.org/10.1115/1.4041197.

Zare, V., 2015. A comparative exergoeconomic analysis of different ORC configurations for binary geothermal power plants. Energy Convers. Manag. 105, 127–138. http://dx.doi.org/10.1016/j.enconman.2015.07.073.

Zhang, J., Qin, K., Li, D., Luo, K., Dang, J., 2020. Potential of Organic Rankine Cycles for unmanned underwater vehicles. Energy 192, 116559. http://dx.doi.org/10.1016/j.energy.2019.116559.

Zhou, J., Zhang, C., Su, S., Wang, Y., Hu, S., Liu, L., Ling, P., Zhong, W., Xiang, J., 2018. Exergy analysis of a 1000 MW single reheat supercritical CO2 Brayton cycle coal-fired power plant. Energy Convers. Manag. 173, 348–358. http://dx.doi.org/10.1016/j.enconman.2018.07.096.